1-1-2014

Multilevel Design Optimization and the Effect of Epistemic Uncertainty

Benjamin Edward Nesbit

Multilevel design optimization and the effect of epistemic uncertainty

By

Benjamin Edward Nesbit

A Thesis
Submitted to the Faculty of
Mississippi State University
in Partial Fulfillment of the Requirements
for the Degree of Master of Science
in Aerospace Engineering
in the Department of Aerospace Engineering

Mississippi State, Mississippi

December 2014

Multilevel design optimization and the effect of epistemic uncertainty

By

Benjamin Edward Nesbit

Approved:

_____

Masoud Rais-Rohani
(Major Professor)

_____

Thomas E. Lacy
(Committee Member)

_____

Ratneshwar Jha
(Committee Member)

_____

J. Mark Janus
(Graduate Coordinator)

_____

Jason M. Keith
Interim Dean
Bagley College of Engineering

Name: Benjamin Edward Nesbit

Date of Degree: December 13, 2014

Institution: Mississippi State University

Major Field: Aerospace Engineering

Major Professor: Masoud Rais-Rohani

Title of Study: Multilevel design optimization and the effect of epistemic uncertainty

Pages in Study: 101

Candidate for Degree of Master of Science

This work presents the state of the art in hierarchically decomposed multilevel optimization. This work is expanded with the inclusion of evidence theory with the multilevel framework for the quantification of epistemic uncertainty. The novel method, Evidence-Based Multilevel Design optimization, is then used to solve two analytical optimization problems. This method is also used to explore the effect of the belief structure on the final solution. A methodology is presented to reduce the costs of evidence-based optimization through manipulation of the belief structure. In addition, a transport aircraft wing is also solved with multilevel optimization without uncertainty. This complex, real world optimization problem shows the capability of decomposed multilevel framework to reduce costs of solving computationally expensive problems with black box analyses.

ACKNOWLEDGEMENTS

I would like to thank my research group for their help in this process. Dr. Masoud Rais-Rohani's guidance has been invaluable in this process pushing me forward in my work, but also supporting me in the weeks when things went wrong. I would not have completed this work without Dr. Saber DorMohammadi's help in understanding these techniques. Dr. Jeff Parrish was invaluable in helping me through the computer programming required for this work.

I would like to thank my parents for their love and encouragement both in raising me and in supporting me in my passion for aviation. I would also like to thank my loving and supportive wife who has encouraged me through the daily stresses and struggles of this degree.

The financial support for this work was provided by the Mississippi State University's Bagley College of Engineering and Raspet Flight Research Laboratory.

TABLE OF CONTENTS

ACKNOWLEDGEMENTS ii

LIST OF TABLES v

LIST OF FIGURES vi

CHAPTER

I. INTRODUCTION 1

Previous Work 3

II. DECOMPOSED MULTILEVEL OPTIMIZATION 8

An Example of Convergence Using Different Solution Strategies 15

III. OPTIMIZATION UNDER UNCERTAINTY 20

Reliability Based Design Optimization 20
Non-Deterministic Design Optimization Techniques for Epistemic Uncertainty 22

IV. EPISTEMIC UNCERTAINTY AND EVIDENCE THEORY 24

V. EVIDENCE-BASED MULTILEVEL DESIGN OPTIMIZATION 31

VI. MULTILEVEL OPTIMIZATION WITH UNCERTAINTY 44

Formulation of Example Problems 44
Problem 1 44
Problem 2 49
On the Effect of Belief Structure 52
Replicating Results with Different Belief Structures 56
Decreasing Costs through Manipulation of Belief Structures 59

VII. MULTILEVEL OPTIMIZATION OF A TRANSPORT AIRCRAFT WING 62

Element 11: System-Level Structural Model and Design 67

Element 22 and 33: Macro-Level Structural Design and Buckling Model 74
Element 34 and 35: Micro-Level Material Model Analysis and Design 82
Optimization Framework and Results 85

VIII. CONCLUSIONS AND FUTURE WORK 93

REFERENCES 96

LIST OF TABLES

2.1 Convergence of single loop optimization....18

2.2 Convergence of double loop optimization....19

6.1 Summary of results of Problem 1....48

6.2 Summary of results from problem 2. 52

6.3 Raw optimum solutions for various belief structures....55

6.4 Solutions with weighted mean as point estimate for various belief structures 56

6.5 Results from belief structures with same Cumulative Plausibility Structure 58

6.6 Results of belief structure in Figure 6.8 showing reduced cost metrics....61

7.1 Transport Aircraft and Wing Specifications 70

7.2 Material Properties for Wing Components 73

7.3 Material Properties for Face Sheet Components....78

7.4 Material Properties for Enhanced Matrix Components....84

7.5 Design variable values for Element 11 89

7.6 Design variable values of the optimized panels....90

7.7 Target and response values for the transport aircraft wing problem....92

LIST OF FIGURES

2.1 Example of a hierarchically decomposed multilevel system 9

2.2 Graphical depiction of solution strategies 14

2.3 Two bar truss free body diagram.....16

2.4 Hierarchical decomposition of the two bar truss problem 17

4.1 Examples of belief structure forms 25

4.2 A general belief structure 26

4.3 Contributing belief structures for the joint belief structure in Figure 4.4 28

4.4 Joint belief structure of x1 and x2 with constraint boundary shown.....28

5.1 Diagram of the flow of information for EBMLDO.....35

5.2 Target-response coordination for characteristic numbers with $Pa = 0$.....37

5.3 Target-response coordination for characteristic numbers with $Pa > 0$.....38

5.4 Structure used to validate characteristic numbers' target-response process.....39

5.5 Belief structures used to test characteristic numbers for $Pa > 0$.....42

6.1 Belief structure used for Problem 1.....45

6.2 Hierarchical decomposition of Problem 1 in Chapter 2 with uncertainty.....46

6.3 Hierarchical decomposition of Problem 2.....50

6.4 Belief structure used for problem 2.....51

6.5 Belief structures tested to determine their effect.....53

6.6 Comparison of the cumulative plausibility functions for tested belief structures 57

6.7 The belief structure with the same cumulative plausibility structure from the left side as the original belief structure from problem 1. 58

6.8 Belief structure which reduces costs while giving the same optimal point.....60

7.1 The multiple levels optimized in the transport aircraft wing problem. 64

7.2 The decomposed framework showing the three levels of the transport aircraft wing problem, the corresponding inputs, and the variables 65

7.3 Two panel group decomposition of the Transport Aircraft Wing Problem 66

7.4 The finite element model of the wing 68

7.5 Normalized chordwise lift distribution 69

7.6 Normalized spanwise lift distribution 70

7.7 Graphical definition of variables in the middle level 74

7.8 Comparison of the original panel 1 and its rectangular approximation 76

7.9 Hierarchical decomposition of the two section transport wing problem.....85

7.10 The VisualDOC workflow for the Transport Aircraft Wing Optimization.....86

CHAPTER I

INTRODUCTION

As computational capabilities have matured, there has been a greater focus on engineering design optimization. Optimization has always been a computationally costly proposition as it requires multiple analyses of a problem, but in recent years, the analyses have become increasingly complex with the addition of more high cost "black box" analyses such as finite element analysis and computational fluid dynamics analysis. The high costs have led to a focus on improving the efficiency of solving a problem. Decomposed multilevel optimization is one way to reduce the costs of the problem (Kim et al. 2003).

Multilevel design optimization has been explored as a means to manage complex design problems by breaking the large problem into several smaller optimization problems. The cost advantages of the decomposition come from the separation of the complex analyses. Though more total function calls are needed for a solution, fewer analyses are needed because each function call is not running all the analyses but a subset. Decomposition also allows isolation of features that may require the problem to use a less efficient optimization algorithm (Kim et al. 2003). This allows the other elements to use the most computationally efficient algorithm, while the element containing the trouble features uses an algorithm suited to its needs. In the all-in-one problem, the entire problem would have to use the less efficient optimization technique.

The decomposition adds costs in the optimization framework to reduce costs of the total analysis. Therefore, there is a cost penalty when low cost analyses are analyzed (such as the ones considered in Chapters 2 and 6), but costs are drastically reduced when high cost analyses are considered.

Decomposition of a problem is especially useful when natural divisions exist in the original problem. Design variables can then be isolated in separate optimization sub-problems. The source of the added cost in the optimization framework is that often optimization of one sub-problem will lead to solutions that are adverse to another. Thus, careful coordination is needed to ensure a cohesive and balanced final result.

Uncertainty analysis has also become increasingly important in recent years. Advances in optimization have led to more efficient designs, but these designs sometimes fail when uncertainty is not properly considered. For instance, a design that would be on the point of failure if machined exactly to specification or thicker, with a material that is as strong or stronger than the assumed material, would fail if either of those assumptions were not met. Of course, in industry, a mere specification is not used for machinist drawings, but a tolerance. Uncertainty quantification gives a likelihood of failure of a design within certain tolerances and with a material which has a distribution for material properties. This quantification can then be used in an optimization framework to optimize the structure subject to a certain probability that the structure will fail. This type of optimization allows for more optimal solutions while still ensuring a reliable product.

Typically, uncertainty is considered in two different forms: aleatory and epistemic. Aleatory uncertainty is the natural variation in a system. It is sometimes referred to as irreducible uncertainty because the uncertainty cannot be reduced without

changing the system. Aleatory uncertainty is quantified using probability distributions such as a Normal distribution (bell curve), Weibull distribution, Uniform distribution, etc. Epistemic uncertainty is due to a lack of knowledge of the system. It is sometimes called reducible uncertainty because the bounds of the uncertainty can be reduced as more knowledge of the system is gained. For example, if there is no knowledge of a system, no one can say what the value of a certain parameter is. But the value of that parameter for that system can be guessed if there is knowledge of the type of the system. A general interval for the parameter can be hypothesized by comparing this system to similar systems, adding a margin of error in consideration of how this system varies from those known. By running experiments, samples are gathered giving an incomplete, but more certain idea about the parameter's magnitude. With further experiments, experts can give more certain intervals of the parameter's value and its likelihood of being in each interval. If enough experimental evidence is gathered, an accurate probability distribution can be formed, at which point the uncertainty would be aleatory and irreducible.

Uncertainty quantification adds computational costs to any system. No longer is any variable a mere value, but a distribution or an interval structure requiring multiple values to accurately quantify. The accurate combination and propagation of these multiple values adds to the computational costs and may require multiple function calls to ascertain. Thus, any way to reduce computational costs would be beneficial to offset the addition costs incurred by consideration of uncertainty.

Previous Work

Multilevel design optimization with analytical target cascading (ATC) was first proposed by Michelena et al. (1999). This work used consistency constraints to ensure

convergence. Kim et al. (2003) proposed a relaxed formulation of target cascading in which the summation of inconsistencies between targets and responses at a certain level are added to the objective function at that level to encourage convergence. This simple linear penalty function was inadequate, so it was replaced by more complex penalty functions. Michalek and Papalambros (2005) used a quadratic penalty function which multiplied the inconsistencies by a weight factor before squaring them. This weight factor allowed the penalty to be better matched to the objective function at the beginning of the optimization and increased as the optimization proceeded. Kim et al. (2006) proposed the use of a Lagrangian penalty function. This penalty used a Lagrangian multiplier to increase the penalty on the simple linear penalty. Tosserams et al. (2006) combined the quadratic and Lagrangian penalties to form an augmented Lagrangian penalty that possessed the advantages of each penalty function. DorMohammadi and Rais-Rohani (2013) proposed the use of an augmented Lagrangian with exponential penalty function which uses the normal exponential of the inconsistencies multiplied by weights and Lagrangian multipliers as the penalty function.

Analytical target cascading has been used to solve several engineering problems. Kim et al. (2002) used ATC with variable linear consistency constraint to optimize a simple model of a class VI truck. Louca et al. (2002) used ATC with variable consistency constraint in the optimization of an advanced ground vehicle. Allison et al. (2005) used ATC with a quadratic penalty to optimize the design of an electric water pump. Allison et al. (2006) solved a simple aircraft design problem using ATC with a quadratic penalty. In 2007, Tosserams et al. solved a speed reducer using ATC with an Augmented Lagrangian

penalty function. DorMohammadi et al. (2014) used ATC with an exponential penalty function to optimize a sandwich composite plate reinforced with carbon nano-fibers.

Klir and Smith (2001) showed that evidence theory to be more general than other methods of quantifying epistemic uncertainty. Evidence theory was first proposed by Demster in 1968. Shafer refined it into the theory we know today in 1976. Thus, evidence theory is often referred to as Demster-Shafer Theory or Demster-Shafer theory of evidential reasoning. While evidence theory saw use in artificial intelligence and other fields, it has only recently been used in engineering. Bae et al. (2004) compared evidence theory, possibility theory, and classical probability theory in the prediction of deflection of a three bar truss finite element model. Vasile (2005) used evidence theory in the preliminary planning of a simulated space mission to quantify certain parameters that are not well defined. Bae et al. (2006) used evidence theory in prediction of tip deflection of a finite element model of a simulated wing.

Uncertainty quantification and engineering design optimization have been combined using several different uncertainty quantification methods. Enevoldsen and Sorensen (1994) first applied statistical analysis to the optimization of structures. Tu et al. (1999) presented a new method for RBDO which reduced costs over earlier efforts. Nikolaidis et al. (2004) demonstrated design optimization using possibility theory in possibility based design optimization (PBDO). Agarwal et al. (2004) integrated evidence theory and design optimization. Mourelatos and Zhou (2006) formalized the use of evidence theory in design optimization in a method called evidence based design optimization (EBDO). Youn et al. (2006) used Bayesian theory in design optimization in a method known as Bayesian reliability based design optimization (BRBDO).

Du and Chen (2002) used RBDO in the optimization of a car's side structure against impact. Choi et al. (2004) extended Du and Chen's 2002 work by using PBDO to solve the car side impact problem. McDowell (2007) explored the use of RBDO in integrated computational materials engineering (ICME). Youn et al. (2007) used PBDO in the design of a piston-cylinder system. In 2012, Salehghaffari and Rais-Rohani used evidence theory in the optimization of a cylinder under compression with uncertain material properties. Rouhi and Rais-Rohani (2013) used RBDO in the optimization of a nano reinforced composite cylinder under compressive loads.

While reliability based design optimization and multilevel design optimization are both fairly common now, little has been done on combining them. Kokkolaras et al. (2004) combined ATC using a quadratic penalty with RBDO propagating the uncertain targets and responses using first and second moment matching (matching the mean and standard deviation of the uncertain targets to the responses assuming a normal distribution). Liu et al. (2006) used probabilistic ATC with a linear penalty to solve the piston and cylinder problem later solved the Youn et al. (2007) using PBDO. DorMohammadi and Rais-Rohani (2012) combined ATC with an augmented Lagrangian penalty and RBDO to solve a number of analytical problems with first and second moment matching. To the author's knowledge, no one has combined an epistemic uncertainty quantification technique with multilevel optimization.

Much work has been performed in the area of multilevel design optimization, yet those in industry still consider it immature. Several obstacles stand in the way of multilevel optimization's use in industry. The goal of this work was to find solutions to two of these obstacles, namely the need to address epistemic uncertainty within the

multilevel framework and the need for a "real world" example problem solved in the multilevel framework.

The remainder of this thesis is organized as follows: Chapter 2 gives a description of multilevel optimization and gives an example of its use. Chapter 3 gives a description of optimization under uncertainty and the principles of reliability-based design optimization. Chapter 4 gives a description of epistemic uncertainty and how evidence theory quantifies that uncertainty. Chapter 5 gives a description of a new method of multilevel optimization with evidence theory based uncertainty quantification. Chapter 6 gives the solution of several problems with epistemic uncertainty and explores the effect of belief structure on the solution. Chapter 7 contains the description of a transport aircraft wing optimized without uncertainty and gives the results of this problem. Chapter 8 gives a summary of the research findings and suggestions of future work in this area.

CHAPTER II

DECOMPOSED MULTILEVEL OPTIMIZATION

Decomposed multilevel optimization is the process of dividing a single large optimization problem into multiple smaller, easier to solve problems called elements. The goal of this separation is to isolate costly analyses into an element, so their cost is incurred less often. The element ij represents the j^{th} element in i^{th} level of the hierarchy as shown in Figure 2.1. Analytical Target Cascading (ATC) is one of several methods that can be used to coordinate the element solutions to meet the system-level targets (Michelena et al. 1999). In ATC, the hierarchy is established using a single top-level element to coordinate the system. The target value, $\boldsymbol{t}_{ij}$, emanates from the parent level of element ij. The corresponding response value, $\boldsymbol{r}_{ij}$, comes from element ij in the level below the parent. A consistency constraint, $\boldsymbol{c}_{ij} = \boldsymbol{t}_{ij} - \boldsymbol{r}_{ij}$, defines the amount of agreement between a target and the corresponding response value. The local decision variables in element ij are defined by vector $\bar{\boldsymbol{x}}_{ij}$ which includes a subset of the global design variable vector $\boldsymbol{X}$ along with added variables $\boldsymbol{t}_{(i+1)k}$ and $\boldsymbol{r}_{ij}$ should those values be needed (Kim et al. 2003). The children, $\boldsymbol{D}_{ij}$, of a parent element are the elements on a lower level than the parent element with which the parent element shares information. In Figure 2.1, the children of Element 22 are Element 3(n+1) and Element 3(n+2). Elements can only communicate with their parent, grandparent, children, or grandchildren elements

and cannot communicate directly with an element outside its hierarchy. Using the example in Figure 2.1, Element 3(n+1) can communicate with Element 22 and Element 11 directly, but cannot directly communicate with any other element in the hierarchy.

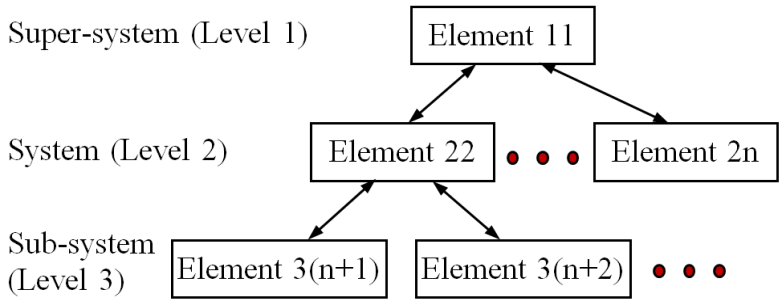

Figure 2.1 Example of a hierarchically decomposed multilevel system

The decomposition of the original problem can follow different forms. For instance, an aircraft optimization problem might be decomposed along separate design aspects or components focused on wings, fuselage, empennage, and engine with each physical component optimized in light of the full aircraft's goals. Another form of decomposition divides the problem along different disciplines. An example using the same aircraft would be to decompose the system into aerodynamics, structures, flight controls, and propulsion (Kim et al. 2003). In that case, the parent element for the optimization would be the aircraft level element. The hierarchy does not have to end at the component level as further structural, aerodynamic, and systems decomposition is possible for each component.

To decompose a problem, its objective function must be separable, and the constraints must not require excessive shared information. Separability is easily obtained

if the objective function is the sum of several components that can be distributed to different elements in the decomposition. Each component is individually optimized with the knowledge that the system will be at optimum when each component is optimum while still satisfying the consistency constraints. Using the example discussed above, the empty weight of an aircraft is merely the sum of its components' weights. Separability is more difficult or impossible if the objective function is not a summation.

The requirement that constraints not require excessive information means that the constraints must be compartmentalized in the decomposition. They may depend on shared information, but should not be a function of a large amount of shared data. This requirement arises from the source of complexity in the multilevel framework, namely the coordination of targets and responses. (Kim et al. 2003)

For most optimization problems, the computational costs depend heavily on the complexity of the function evaluations. In decomposed multilevel optimization, the coordination also contributes to the computational costs. Thus, decomposition of an optimization problem involving simple analytical functions may increase computational costs. On the other hand, if an optimization problem with computationally expensive functions, such as "black box" analysis tools, is decomposed, then it is possible to reduce the computational costs by a considerable amount through a decomposed multilevel approach with proper coordination and solution strategy (DorMohammadi et al. 2014).

The key to any decomposed optimization is careful coordination of targets and responses to ensure that the final result is valid. Because the target and associated response represent the same quantity in the non-decomposed all-at-once problem, they must be equal in any valid decomposed solution. Several methods have been used to

coordinate these terms. Michelena et al. (1999) used a constraint in each element that targets and responses be within a certain tolerance (i.e., $\boldsymbol{c}_{ij} \cong 0$). This formulation for element ij is expressed as

$$\begin{aligned} &\min_{\bar{\boldsymbol{x}}_{ij}} f_{ij}(\bar{\boldsymbol{x}}_{ij}) + \boldsymbol{\varepsilon}_{ij} \\ &s.t. \quad \boldsymbol{g}_{ij}(\bar{\boldsymbol{x}}_{ij}) \leq 0 \\ &\boldsymbol{h}_{ij}(\bar{\boldsymbol{x}}_{ij}) = 0 \\ &\|\boldsymbol{c}_{ij}\| = \|\boldsymbol{t}_{ij} - \boldsymbol{r}_{ij}\| \leq \boldsymbol{\varepsilon}_{ij} \end{aligned} \tag{2.1}$$

where $\bar{\boldsymbol{x}}_{ij} = [\boldsymbol{x}_{ij}, \boldsymbol{r}_{ij}, \boldsymbol{t}_{ij}, \boldsymbol{t}_{(i+1)k_1}, \dots, \boldsymbol{t}_{(i+1)k_{D_{ij}}}]$

where f_{ij} is the function being optimized in element ij, $\boldsymbol{g}_{ij}$ is the vector of all inequality constraints, $\boldsymbol{h}_{ij}$ is the vector of all equality constraints, and $\boldsymbol{x}_{ij}$ is the vector of all local design variables which belong solely to element ij. Unfortunately, the formulation in Eq. (2.1) slows exploration of the design space because the target and response are permanently bound to each other within the set tolerance $\boldsymbol{\varepsilon}_{ij}$ and large weights are needed for the penalty added to the objective function to force convergence. This means the choice of initial design point can have a great influence on the optimization result and its convergence.

Thus, most coordination strategies use a relaxed formulation in which a term is added to the objective function to penalize each element according to the difference between target and response (Kim et al. 2003). Using this strategy, Element ij is formulated as

$$\min_{\bar{\boldsymbol{x}}_{ij}} f_{ij}(\bar{\boldsymbol{x}}_{ij}) + \pi(\boldsymbol{c}_{ij}, \boldsymbol{c}_{(i+1)k_1}, \dots, \boldsymbol{c}_{(i+1)k_{D_{ij}}})$$

$$s.t. \quad \boldsymbol{g}_{ij}(\bar{\boldsymbol{x}}_{ij}) \leq 0 \qquad (2.2)$$

$$\boldsymbol{h}_{ij}(\bar{\boldsymbol{x}}_{ij}) = 0$$

where $\bar{\boldsymbol{x}}_{ij} = [\boldsymbol{x}_{ij}, \boldsymbol{r}_{ij}, \boldsymbol{t}_{ij}, \boldsymbol{t}_{(i+1)k_1}, \dots, \boldsymbol{t}_{(i+1)k_{D_{ij}}}]$

where π represents the penalty function. The penalty function should be small for small inconsistencies, but increase rapidly for large inconsistencies. Several penalty function formulations have been developed including quadratic penalty (Michalek and Papalambros 2005), ordinary Lagrangian penalty (Kim et al. 2006), augmented Lagrangian penalty (Tosserams et al. 2006), and exponential penalty (DorMohammadi and Rais-Rohani 2013). Quadratic penalty function uses a weight factor to increase the penalty of inconsistencies through the optimization. Lagrangian penalty function uses an updating Lagrangian multiplier to modify the penalties in a more adaptive way. Augmented Lagrangian penalty function sums these two methods to create a penalty function which is both adaptive and able to steadily increase through the optimization process. Hybrid penalty functions, like the Augmented Lagrangian, capture the advantages of each penalty function, allowing them to be more useful.

The exponential penalty function (EPF) formulation is also a hybrid penalty function but uses a different function. The base function $\psi(y) = e^y - 1$ is used for target-response coordination, instead of the simple quadratic function used in quadratic or Augmented Lagrangian penalty functions. Unlike a quadratic function, the exponential formulation is monotonic meaning the equality constraint $\boldsymbol{c}_{ij} = \boldsymbol{t}_{ij} - \boldsymbol{r}_{ij}$ must be

replaced with two inequality constraints $\boldsymbol{c}_{ij} \leq \boldsymbol{t}_{ij} - \boldsymbol{r}_{ij}$ and $\boldsymbol{c}_{ij} \geq \boldsymbol{t}_{ij} - \boldsymbol{r}_{ij}$ to achieve a balanced penalty. The objective function using EPF for element ij is formulated as

$$\min_{\bar{\boldsymbol{x}}_{ij}} f_{ij}(\bar{\boldsymbol{x}}_{ij}) + \left\{\frac{\boldsymbol{\mu}_{ij}}{\boldsymbol{a}_{ij}}\left[e^{\boldsymbol{a}_{ij}(\boldsymbol{t}_{ij}-\boldsymbol{r}_{ij})} - 1\right] + \frac{\boldsymbol{\gamma}_{ij}}{\boldsymbol{b}_{ij}}\left[e^{\boldsymbol{b}_{ij}(\boldsymbol{r}_{ij}-\boldsymbol{t}_{ij})} - 1\right]\right\} +$$

$$\sum_{k\in D_{ij}} \left\{\frac{\boldsymbol{\mu}_{(i+1)k}}{\boldsymbol{a}_{(i+1)k}}\left[e^{\boldsymbol{a}_{(i+1)k}(\boldsymbol{t}_{(i+1)k}-\boldsymbol{r}_{(i+1)k})} - 1\right] + \frac{\boldsymbol{\gamma}_{(i+1)k}}{\boldsymbol{b}_{(i+1)k}}\left[e^{\boldsymbol{b}_{(i+1)k}(\boldsymbol{r}_{(i+1)k}-\boldsymbol{t}_{(i+1)k})} - 1\right]\right\} \quad (2.3)$$

where $\boldsymbol{\mu}_{ij}$, $\boldsymbol{\gamma}_{ij}$, $\boldsymbol{\mu}_{(i+1)k}$, and $\boldsymbol{\gamma}_{(i+1)k}$ are multipliers, $\boldsymbol{a}_{ij}$, $\boldsymbol{b}_{ij}$, $\boldsymbol{a}_{(i+1)k}$, and $\boldsymbol{b}_{(i+1)k}$ are weight factors, and $\boldsymbol{D}_{ij}$ is the set of all children of element ij. For the formulation considered in this study, the multipliers are updated using the formulas $\boldsymbol{\mu}_{ij}^{n+1} = \boldsymbol{\mu}_{ij}^{n} e^{\boldsymbol{a}_{ij}^{n}(\boldsymbol{t}_{ij}^{n}-\boldsymbol{r}_{ij}^{n})}$ and $\boldsymbol{\gamma}_{ij}^{n+1} = \boldsymbol{\gamma}_{ij}^{n} e^{\boldsymbol{b}_{ij}^{n}(\boldsymbol{r}_{ij}^{n}-\boldsymbol{t}_{ij}^{n})}$ and the weight factors are updated as $\boldsymbol{a}_{ij}^{n+1} = \beta\, \boldsymbol{a}_{ij}^{n}$ and $\boldsymbol{b}_{ij}^{n+1} = \beta\, \boldsymbol{b}_{ij}^{n}$ where $\beta \geq 1$ if $\boldsymbol{c}_{ij}^{n} > \lambda\, \boldsymbol{c}_{ij}^{n-1}$ with n denoting the current iteration. The updating of the weight factors increases the penalty of uncoordinated targets and responses as the process continues. This study looked at both single-loop and double-loop coordination strategies (DorMohammadi and Rais-Rohani 2013).

In the single-loop strategy, the multipliers and weight factors are updated in every iteration as shown in Figure 2.2 (a). This updating approach causes the weights to increase faster and the multipliers to be more responsive. This leads to faster convergence, but sometimes can cause premature convergence if the problem is not well behaved and the weights become too large to allow for continued optimization.

The double loop strategy updates the multipliers and weight factors only after convergence of the inner loop, defined as $\left\|\sum f^{n}(\bar{\boldsymbol{x}}_{ij}) - \sum f^{n-1}(\bar{\boldsymbol{x}}_{ij})\right\| \forall\, ij \; < \tau$, is found for the current set of multipliers and weight factors. This is depicted in Figure 2.2 (b). Because the weights and multipliers are updated less often, the solutions are

computationally more expensive but less prone to premature convergence and are affected less by changes in the initial weights and the updating factor. For both formulations, convergence is said to be achieved when $\left\|\boldsymbol{c}_{ij}^{n} - \boldsymbol{c}_{ij}^{n-1}\right\| < \tau$ where $\|a\|$ denotes the absolute value of a and τ is the convergence tolerance.

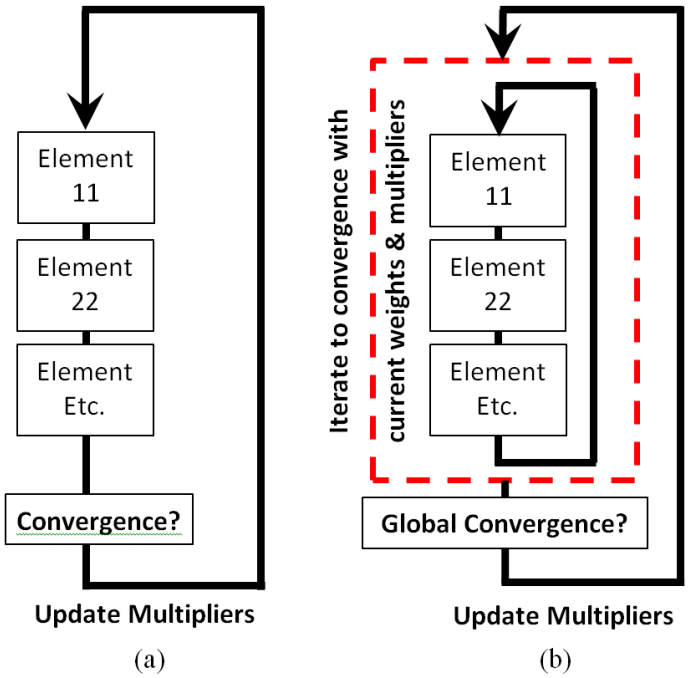

Figure 2.2 Graphical depiction of solution strategies

(a) Single loop
(b) Double loop

In order for the target-response interaction to work, the targets and responses need to be normalized. Normalization allows for the same relative weight to be placed on all discrepancies regardless of the scale of the actual response quantities. It also allows the updating of multipliers to work properly. Normalization can be achieved in two ways: by using some normalization scheme or by manipulating units to give roughly normalized variables. The normalization scheme used here is defined as

$$t_{ij}^{N} = \frac{t_{ij} - t_{ij}^{L}}{t_{ij}^{U} - t_{ij}^{L}} \quad ; \quad r_{ij}^{N} = \frac{r_{ij} - r_{ij}^{L}}{r_{ij}^{U} - r_{ij}^{L}} \tag{2.4}$$

where superscripts N, L, and U refer to normalized, upper, and lower values respectively. Though not explicitly denoted, the normalized values are used in all calculations of penalty functions, updating of parameters, and convergence criteria.

The updating of multipliers relies heavily on a normalized consistency constraint. The multipliers increase the penalty on discrepancies in an asymmetric fashion, "pushing" the target one direction and the response the opposite direction to facilitate convergence. But if these multipliers are incorrectly updated, the multipliers will "push" the targets and responses past convergence. Upon the next update of the multipliers, their values will reverse causing them to be "pushed" back past each other. In these cases, a divergent oscillation occurs between the target and response preventing convergence.

An Example of Convergence Using Different Solution Strategies

The two bar truss problem shown in Figure 2.3 was solved to demonstrate the method and shows the differences between the loop strategies. This system is optimized for minimum weight under the specified load subject to an upper bound constraint on the axial stress in each bar as well as side constraints on the design variables defined by vector z.

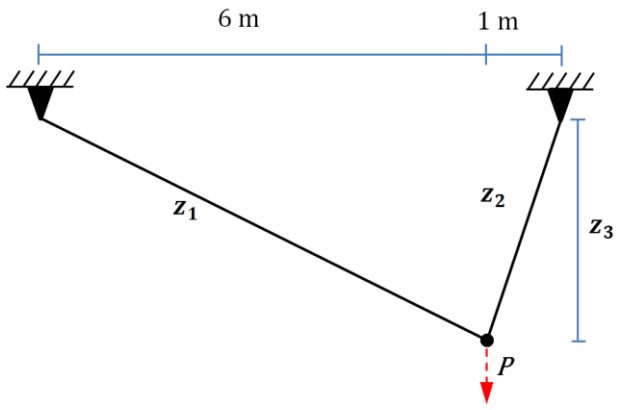

Figure 2.3 Two bar truss free body diagram

The deterministic all-at-once (AAO) formulation of the optimization problem is expressed as (Rao 1996)

$$\begin{aligned} &\min_{\mathbf{z}} \; f = \rho \left(z_1 \sqrt{z_3^2 + 36} + z_2 \sqrt{z_3^2 + 1} \right) \\ &\text{s.t.} \quad g_1 = \frac{P \sqrt{z_3^2+36}}{7\, \sigma_0\, z_3\, z_1} - 1 \leq 0 \\ &\qquad g_2 = \frac{6\, P \sqrt{z_3^2+1}}{7\, \sigma_0\, z_3\, z_2} - 1 \leq 0 \\ &0 \leq z_1 \leq 0.1\,; \;\; 0 \leq z_2 \leq 0.1; \; 1 \leq z_3 \leq 6 \end{aligned} \tag{2.5}$$

where design variables z_1 and z_2 are the areas of bars 1 and 2, respectively, z_3 is the truss height, with specific weight $\rho = 76{,}500 \ \mathrm{N/m^3}$, applied force $P = 1{,}000$ N and allowable axial stress $\sigma_0 = 10^5$ Pa. The optimum point reported in literature is $[z_1^*, z_2^*, z_3^*] = [\ 0.003779\ \mathrm{m^2},\ 0.0092579\ \mathrm{m^2}, 2.45\ \mathrm{m}]$ where $f^* = 3747.7$ N and both constraints are active.

This problem is decomposed into two elements in a two-level hierarchy as shown in Figure 2.4. Each element optimizes one of the bars in the truss while z_3 is shared between the two elements.

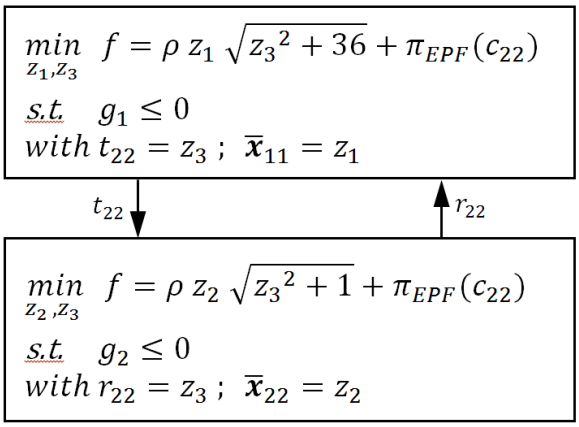

$$\pi_{EPF}(c_{22}) = \{\frac{\mu_{22}}{a_{22}}\left(e^{a_{22}\,(t_{22}-r_{22})} - 1\right) + \frac{\gamma_{22}}{b_{22}}\left(e^{b_{22}\,(r_{22}-t_{22})} - 1\right)\}$$

Figure 2.4 Hierarchical decomposition of the two bar truss problem

The problem was first solved using the single loop formulation with initial weights equal to 1, with $\beta = 1.1$, and $\tau = 0.0001$. Several iterations of the solution are shown in Table 2.1 below. It should be noted that t_{22} and r_{22} represent the target and response values for design variable z_3 The initial values are denoted as iteration 0. The values of the objective function are given with the penalty function included.

Table 2.1 Convergence of single loop optimization

Iteration	t_{22} (m)	r_{22} (m)	z_1 (m^2)	z_2 (m^2)	f (N)	c_{22}	a_{22}
0	1.00	1.00	0.10000	0.10000	57,351.87	0.000000	1
1	4.94	1.04	0.00225	0.01189	2,745.81	3.904456	1
2	2.96	1.29	0.00323	0.01084	3,510.12	1.669229	1
3	2.19	1.73	0.00416	0.00990	4,111.16	0.460620	1.1
4	2.16	2.05	0.00422	0.00954	4,018.08	0.110384	1.21
5	2.27	2.23	0.00404	0.00939	3,884.79	0.039446	1.21
6	2.34	2.33	0.00393	0.00933	3,813.98	0.015068	1.33
7	2.39	2.38	0.00387	0.00930	3,781.30	0.006563	1.46
8	2.41	2.41	0.00383	0.00928	3,765.56	0.003102	1.61
9	2.42	2.42	0.00381	0.00927	3,757.61	0.001552	1.77
10	2.43	2.43	0.00380	0.00927	3,753.41	0.000812	1.95
…	…	…	…	…	…	…	…
25	2.4492	2.4492	0.00378	0.00926	3,747.75	1.46 E -6	7.40

Since the initial design point is conservative, there is a large drop in the objective function from the iteration 0 to 1, followed by a rise until iteration 3. This is followed by the slow, consistent fall. This is because by the program finds a non-converged minimum for that set of targets, responses, weights and multipliers. In the next iteration those values have updated, causing the previous solution to be suboptimal, and the algorithm solves again with better convergence. As can be observed below, the difference between iteration 10 and iteration 25 is fairly small, but takes the majority of the computational costs and iterations. In total, this solution took 3.06 seconds and 1,778 function calls.

To show the difference between the single and double loop strategies, the solution was re-run using double loop strategy once again using initial weights of 1, with $\beta = 1.1$, and $\tau = 0.0001$. Several iterations of that solution are shown in Table 2.2. These results show a much more gradual convergence. The inner loop converged after iteration 4 passing the information to the outer loop to update the multipliers. In this case, the

criteria were not met to update the multipliers. The next inner loop convergence occurred after iteration 13. The algorithm moves very little after each update of the weights and multipliers, but this causes a less jumpy solution than the single loop approach. Since there is some level of convergence before the weights and multipliers are updated, the criteria to update the weights are met less often resulting in a solution with lower final weights. In total this solution took 5.31 seconds and 3,559 function calls, an increase of 73 % and 100 % over the single loop formulation, respectively. This shows that the single loop formulation is more computationally efficient than the double loop formulation for this simple problem.

Table 2.2 Convergence of double loop optimization

Iteration	t_{22} (m)	r_{22} (m)	z_1 (m^2)	z_2 (m^2)	f (N)	c_{22}	a_{22}
0	1.00	1.00	0.10000	0.1000	57,351.87	0.000000	1
1	4.94	1.04	0.00225	0.0119	2,745.81	3.904456	1
2	4.96	1.04	0.00224	0.0119	2,744.65	3.921422	1
3	4.96	1.04	0.00224	0.0119	2,744.63	3.921729	1
4	4.96	1.04	0.00224	0.0119	2,744.63	3.921735	1
5	2.95	1.30	0.00324	0.0108	3,516.27	1.657884	1
6	3.09	1.34	0.00312	0.0107	3,471.72	1.748844	1
7	3.11	1.35	0.00310	0.0107	3,465.36	1.764016	1
8	3.13	1.35	0.00315	0.0107	3,495.97	1.772641	1
9	3.12	1.35	0.00301	0.0107	3,463.55	1.768471	1
10	3.12	1.35	0.00301	0.0107	3,463.87	1.767674	1
…	…	…	…	…	…	…	…
66	2.44948	2.44947	0.00378	0.009258	3,747.73	7.39 E -6	1.21

CHAPTER III

OPTIMIZATION UNDER UNCERTAINTY

Reliability Based Design Optimization

Engineering products are not manufactured in a deterministic fashion, nor are engineering materials properly quantified by deterministic specifications. Despite this, most engineering optimizations are deterministic and treat the part dimensions and material specifications as deterministic. This leads to products that may be over-designed with uncharacterized uncertainty, as in the case of A-basis or B-basis values, or have a higher than desired failure rate if mean values are used. In either of these cases, the uncertainty in the system is not considered during the design optimization process.

Uncertainty quantification is needed in the design of products to ensure that parts fit together, components do not fail excessively, and the product works properly. Reliability-Based Design Optimization (RBDO) brings uncertainty quantification into the design optimization process. A standard all-at-once, deterministic optimization problem is formulated as

$$\begin{aligned} \min_{\boldsymbol{x}} \quad & f(\boldsymbol{x}) \\ s.t. \quad & \boldsymbol{g}(\boldsymbol{x}) \leq 0 \\ & \boldsymbol{h}(\boldsymbol{x}) = 0 \end{aligned} \tag{3.1}$$

where $\boldsymbol{x}^l \leq \boldsymbol{x} \leq \boldsymbol{x}^u$

where $\boldsymbol{x}$ is the vector of design variables, $f(x)$ is the objective function to be optimized, $\boldsymbol{g}$ is the vector of all inequality constraints, $\boldsymbol{h}$ is the vector of all equality constraints, and $\boldsymbol{x}^l$ and $\boldsymbol{x}^u$ are the vectors of the upper and lower bounds for $\boldsymbol{x}$.

RBDO changes the deterministic design constraints into probability of failure, P_f, or reliability, $R = 1 - P_f$, constraint formulations depending on whether the focus is on the failure or the safe region of the design space. Expressing the constraints in terms of failure probability changes the formulation of eq. (3.1) to (DorMohammadi & Rais-Rohani 2012)

$$\begin{aligned} &\min_{\boldsymbol{\mu_X},\mathbf{y}} \quad f(\boldsymbol{\mu_X}, \mathbf{y}, \boldsymbol{\mu_P}) \\ &s.t.\ P(\boldsymbol{g}(\boldsymbol{X}, \mathbf{y}, \boldsymbol{P}) > 0) - P_a \leq 0 \\ &\boldsymbol{h}(\boldsymbol{\mu_X}, \mathbf{y}, \boldsymbol{\mu_P}) = 0 \\ &\boldsymbol{\mu}_x^l \leq \boldsymbol{\mu}_x \leq \boldsymbol{\mu}_x^u\ ;\ \mathbf{y}^l \leq \mathbf{y} \leq \mathbf{y}^u \end{aligned} \tag{3.2}$$

where $\boldsymbol{\mu_X}$ is the vector of means of uncertain variables in vector $\boldsymbol{X}$, $\mathbf{y}$ is the vector of deterministic variables, $\boldsymbol{\mu_P}$ is vector the means for uncertain parameters in vector $\boldsymbol{P}$, $P(A)$ is the probability of event A, and P_a is the allowable probability of failure. The term $\boldsymbol{g}(\boldsymbol{X}, \mathbf{y}, \boldsymbol{P})$ represents the limit state function with $\boldsymbol{g}(\boldsymbol{X}, \mathbf{y}, \boldsymbol{P}) < 0$ representing safety and $\boldsymbol{g}(\boldsymbol{X}, \mathbf{y}, \boldsymbol{P}) > 0$ failure. The allowable probability of failure may be fairly high for low quality products with few safety concerns, but for high reliability products, this probability must be kept low. High reliability products cost more, but they are used in applications where the consequences of the product's failure are significant (airplanes, embedded medical devices, etc.). Since statistical analyses are being used, uncertain

variables and parameters are no longer represented by a single value but by multiple discrete values (incomplete information) or a distribution (complete information).

Traditional RBDO utilizes classical probability theory to quantify the uncertainty by representing uncertain variables by known probability distributions. While classical probability theory can be used to quantify aleatory uncertainty (random or inherent variability), it cannot accurately model epistemic uncertainty, which stems from lack of knowledge of the system, its underlying physics, or operating conditions. With epistemic uncertainty, there is not enough information to form a probability distribution; hence, it is more generally represented in interval form. A further discussion of epistemic uncertainty is found in Chapter 4.

One hindrance to the use of RBDO is the added costs associated with uncertainty analysis. To properly quantify the uncertainty, simulation based techniques or probabilistic analyses must be performed. As more sources of uncertainty are combined, these simulations and analyses become more costly. Most formulations assume that all distributions are normal or can be reduced to an equivalent normal that can be characterized by a mean and a standard deviation. This assumption simplifies the problem and reduces the cost of the analyses but they are still quite expensive (Rouhi and Rais-Rohani 2013, DorMohammadi and Rais-Rohani 2012).

Non-Deterministic Design Optimization Techniques for Epistemic Uncertainty

Uncertainty quantification techniques have been used for modeling epistemic uncertainty based on monotone measures (Choquet 1953), fuzzy set theory (Zadeh 1965), evidence theory (Demster 1968, Shafer 1976), Bayesian theory (Winkler 1972, Berger 1985), possibility theory (Dubois and Prade 1988), and information-gap theory (Ben-

Hiam 2001). Some of these techniques have been integrated with the RBDO concept to create non-deterministic design optimization techniques capable of quantifying epistemic uncertainty. These include possibility based design optimization (PBDO) (Nikolaidis et al. 2004), evidence based design optimization (EBDO) (Agarwal et al. 2004, Mourelatos and Zhou 2006), and Bayesian reliability based design optimization (BRBDO) (Youn et al. 2006).

This study focuses on evidence theory, as its ability to quantify interval-based uncertainty without the use of simplifying assumptions makes it desirable for engineering optimization (Klir and Smith 2001). Others have integrated evidence theory into design optimization (Agarwal et al 2004, Bae et al. 2004, 2006, Mourelatos and Zhou 2006, Salehghaffari and Rais-Rohani 2012), but to the author's knowledge none has done so in a multilevel framework. An overview of evidence theory is presented in the next chapter.

CHAPTER IV

EPISTEMIC UNCERTAINTY AND EVIDENCE THEORY

Epistemic uncertainty is generally represented by intervals with each interval having an upper and lower bounds based on expert opinions or scientific experiments. These intervals, taken together, form a belief structure or frame of discernment for the uncertain parameter. Each interval is defined by an upper bound, a lower bound, and an expression of trust or belief defined by basic probability assignment (BPA), denoted as $m(A)$ for interval A. The BPA is assigned by the statistician based on the level of trust in the interval, its source, or its support. An interval where $m(A) > 0$ is called a focal element. The belief structure for a given variable can take several forms: disjoint, nested, or general as depicted by the simple examples in Figure 4.1.

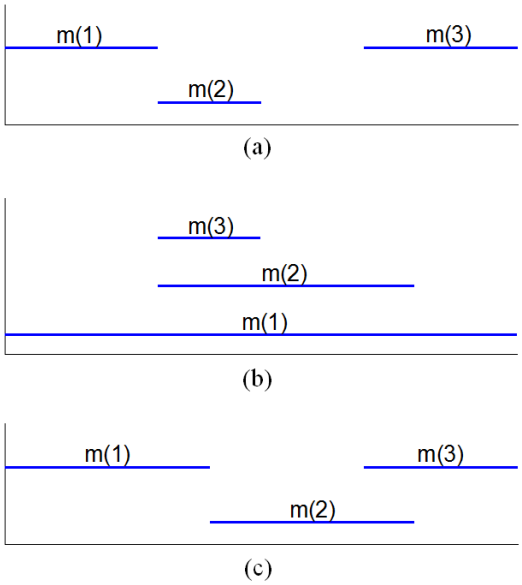

Figure 4.1 Examples of belief structure forms

(a) Disjoint
(b) Nested
(c) General

Evidence theory (ET), also called Dempster-Shafer theory of evidential reasoning, uses two measures of likelihood, belief and plausibility defined respectively as

$$Bel(B) = \sum_{A \subseteq B} m(A) \tag{4.1}$$

$$Pl(B) = \sum_{A \cap B \neq \emptyset} m(A) \quad \forall\, B \subseteq X. \tag{4.2}$$

These measures bound the true probability, $p(B)$, where $Bel(B) \leq p(B) \leq Pl(B)$. The difference between plausibility and belief is the epistemic uncertainty (Demster 1968, Shafer 1976). The smaller the gap is between belief and plausibility, the smaller the epistemic uncertainty. For the example belief structure shown in Figure 4.2, $Bel(3.5 \leq x \leq 7.5) = 0.5$ and $Pl(3.5 \leq x \leq 7.5) = 0.9$, because the bounds $3.5 \leq x \leq 7.5$ completely contain focal elements 3 and 4 while the bounds contain part of focal elements 2 and 5. The epistemic uncertainty for the interval then is $0.9 - 0.5 = 0.4$. It

should be noted that these values for belief and plausibility are valid for all lower bound values between 3 and 4 and all upper bound values between 6 and 7. This property means that the belief and plausibility are stepwise functions. This property holds true for all belief and plausibility functions over the entire domain.

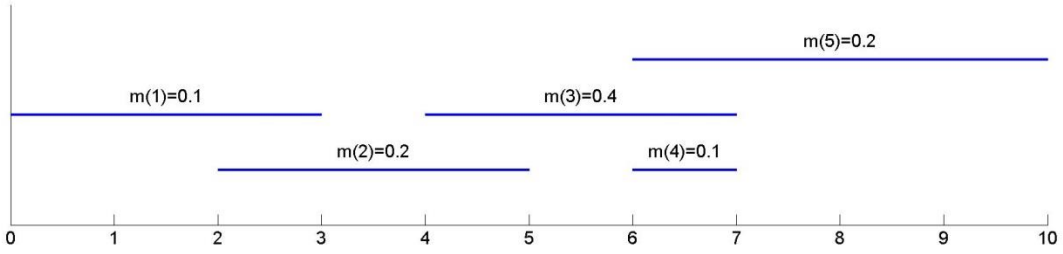

Figure 4.2 A general belief structure

When evidence theory is used to define the belief and plausibility of a function that depends on multiple uncertain variables, the individual belief structures are combined to find the resulting joint belief structure. The number of focal elements in the joint belief structure is found by multiplying (i.e. Cartesian products) the number of focal elements in each contributing belief structure. Hence, each focal element of the joint belief structure takes the form of a hyperspace with the interval bounds being the upper and lower bounds of the contributing focal elements in the original belief structures. If x, y, z represent three uncertain variables with I, J, and K as the number of focal elements, respectively, their joint belief structure can be expressed mathematically as

$$\xi = X \times Y \times Z = \{(x_i, y_j, z_k) | x_i \in X, y_j \in Y, z_k \in Z\}; \quad (4.3)$$

$$m[(x_i, y_j, z_k)] = m[x_i] \times m[y_j] \times m[z_k] \quad (4.4)$$

$$i = 1, \dots, I; \; j = 1, \dots, J; \; k = 1, \dots, K$$

where x_i, y_j, z_k represent the i^{th}, j^{th}, k^{th} focal elements of x, y, z, respectively; $m[x_i]$, $m[y_j]$, and $m[z_k]$ being the BPA of focal element i, j, and k in the belief structure for variable x, y, and z, respectively.

The two disjoint belief structures in Figure 4.3 result in the joint belief structure in Figure 4.4. An arbitrary inequality constraint in the form $g(x1, x2) = x2 - 0.5\, x1^2 + 10\, x1 - 52 \leq 0$ is chosen, where the curve in Figure 4.4 represents the limit state, i.e., $g(x1, x2) = 0$. The belief that the constraint is satisfied is found by adding the BPAs of joint focal elements 11, 12, 13, and 21 or $Bel(g \leq 0) = 0.23$. The plausibility that the constraint is satisfied is $Pl(g \leq 0) = 0.55$ with all the above elements plus elements 22, 23, and 31 contributing. Conversely, the likelihoods of constraint violation are $Bel(g > 0) = 0.45$ and $Pl(g > 0) = 0.77$. This shows that the joint belief structure operates in the same way as any other belief structure.

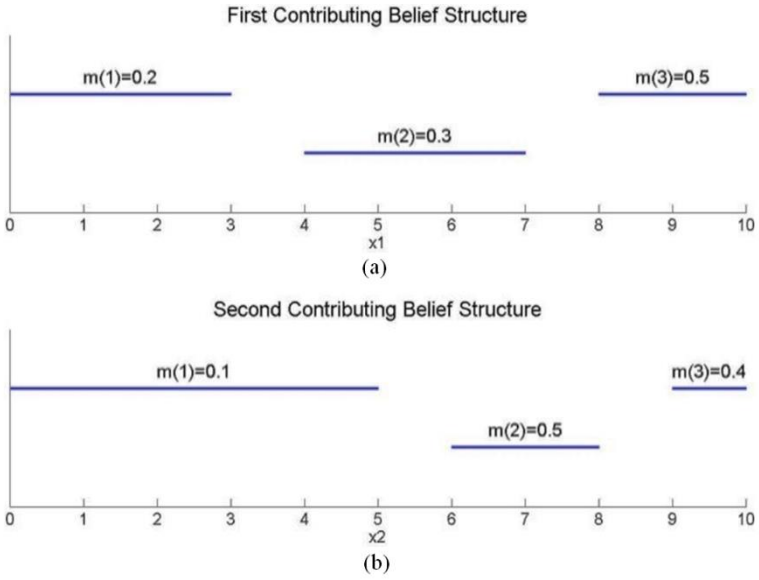

Figure 4.3 Contributing belief structures for the joint belief structure in Figure 4.4

(a) Belief structure for x1
(b) Belief structure for x2

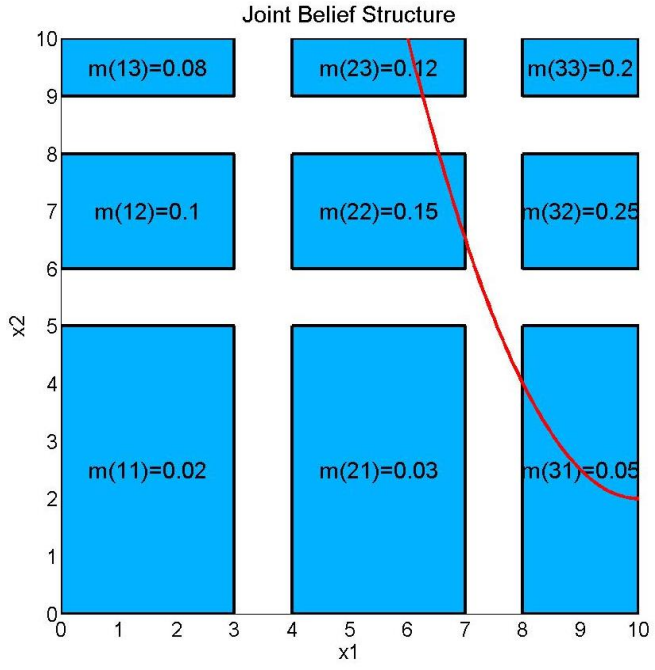

Figure 4.4 Joint belief structure of x1 and x2 with constraint boundary shown

Although the uncertainty bounds for the contributing variables in each joint focal element are known, the upper and lower bounds of the corresponding response function are unknown and need to be calculated as part of the uncertainty propagation step. The upper and lower values of the response function in each focal element are used to describe the corresponding belief structure. For a given set of uncertain variables, there is only one joint belief structure, but the belief and plausibility of different response functions evaluated using that joint belief structure can be drastically different.

Calculating the upper and lower bounds of response functions within each joint focal element is an optimization problem, which can quickly lead to an escalation in computational costs. If the function is continuous and differentiable, a gradient-based optimizer can be used to solve the plausibility sub-optimization problem; otherwise, a gradient-free optimizer must be used. The application of evidence theory to design optimization was explored by Mourelatos and Zhou (2006) and others (Agarwal et al. 2004, Salehghaffari and Rais-Rohani 2012) in what is known as evidence-based design optimization (EBDO). EBDO exploits the property that $Bel(B) + Pl(\neg B) = 1$ to define the belief of a safe design as $Bel(B) = 1 - Pl(\neg B)$ where $Pl(\neg B)$ is the plausibility of failure. The inequality constraints in the deterministic optimization problem (i.e., $g_i \leq 0$) are then converted to failure plausibility constraints (i.e., $Pl(g_i \geq 0) - P_a \leq 0$) in EBDO, where P_a is the maximum allowable failure probability set by the designer. Thus, the final design under uncertainty is guaranteed to have a higher reliability than the minimum allowable as $p(g_i \geq 0) \leq Pl(g_i \geq 0) \leq P_a$.

In this study, the plausibility and belief of failure for a given constraint are found by optimizing the constraint function and the negative of that function while setting side

constraints to the bounds of each joint focal element. This finds the maximum and minimum values of the function in that focal element's hyperspace. If either the maximum or the minimum value violates the constraint, that constraint's BPA contributes to the plausibility of failure. The calculation of failure belief is not needed in this case as the constraint is only on the plausibility, but belief would be calculated by adding the BPA of all focal elements in which both the maximum and minimum values violated the constraint.

CHAPTER V

EVIDENCE-BASED MULTILEVEL DESIGN OPTIMIZATION

The integration of the multilevel optimization framework and uncertainty quantification using evidence theory changes the formulation of the non-deterministic design constraints in each element as well as the manner by which uncertain quantities (i.e., variable or response) are transferred from one element to another in the target-response process of ATC.

When uncertainties are considered, they are introduced in two forms, uncertain parameter vector $\boldsymbol{P}$ and uncertain design variable vector $\boldsymbol{y}$. Here, both uncertain parameters and uncertain variables are represented by a multi-interval belief structure such as that introduced previously in Chapter IV. In this study, each uncertain design variable is viewed as a point estimate, x_i, of the uncertain variable $\boldsymbol{y}_i$ through an algebraic function. This point estimate relationship allows the optimizer to manipulate an entire belief structure of an uncertain variable by changing its point estimate. For this study, the functional relationship is defined as either $\boldsymbol{y}_i = x_i + \boldsymbol{P}_i$ or $\boldsymbol{y}_i = x_i \, \boldsymbol{P}_i$.

A standard optimization problem in element ij has the deterministic formulation

$$\min_{\bar{\boldsymbol{x}}_{ij}} \quad f(\bar{\boldsymbol{x}}_{ij}) + \pi(\boldsymbol{c}_{ij})$$

$$\text{s.t.} \quad \boldsymbol{g}_{ij} \leq 0 \tag{5.1}$$

$$\boldsymbol{h}_{ij} = 0$$

where $\bar{\boldsymbol{x}}_{ij} = [\boldsymbol{x}_{ij}, \boldsymbol{r}_{ij}, \boldsymbol{t}_{ij}, \boldsymbol{t}_{(i+1)k_1}, \dots, \boldsymbol{t}_{(i+1)k_{D_{ij}}}]$ and $\boldsymbol{x}_{ij}^l \leq \boldsymbol{x}_{ij} \leq \boldsymbol{x}_{ij}^u$

with $\boldsymbol{x}_{ij}^l$ and $\boldsymbol{x}_{ij}^u$ representing the lower and upper bounds of the design variables, respectively.

In evidence-based multilevel design optimization (EBMLDO), the deterministic inequality constraints in Eq. (5.1) are converted into non-deterministic inequality constraints on the plausibility of failure, similar to EBDO. A belief structure, like a probability distribution, cannot be properly expressed in an equality constraint. Therefore, equality constraints are evaluated using a single value, the point estimate of the uncertain variables. The side constraints on uncertain design variables must be modified to account for the uncertainty and are enforced on the point estimate of the variable. The EBDO formulation of the element ij optimization problem takes the form

$$\min_{\bar{\boldsymbol{x}}_{ij}} \quad f(\bar{\boldsymbol{x}}_{ij}, \boldsymbol{P}) + \pi(\boldsymbol{c}_{ij})$$

$$s.t. \quad Pl\big(\boldsymbol{g}_{ij} \geq 0\big) - P_a \leq 0 \tag{5.2}$$

$$\boldsymbol{h}_{ij} = 0$$

$$\bar{x}_i^l \leq x_i \leq \bar{x}_i^u$$

where $\bar{x}_i^l$ and $\bar{x}_i^u$ are the modified lower and upper side constraints, respectively, and P_a is the maximum allowable failure probability (Mourelatos and Zhou 2006). For uncertainties of the form $\boldsymbol{y}_i = x_i + \boldsymbol{P}_i$, the modified bounds would be $\bar{x}_i^l = x_i^l -$

$\min(\boldsymbol{P}_i)$ and $\bar{x}_i^u = x_i^u - \max(\boldsymbol{P}_i)$. For uncertainties of the form, $\boldsymbol{y}_i = x_i \, \boldsymbol{P}_i$, the bounds would be modified to $\bar{x}_i^l = x_i^l / \min(\boldsymbol{P}_i)$ and $\bar{x}_i^u = x_i^u / \max(\boldsymbol{P}_i)$. The resulting modified upper and lower bounds have a smaller range than the original upper and lower bounds. This formulation of the constraints allows consideration of epistemic uncertainty within each decomposed element.

In EBMLDO, targets and responses are no longer a single value. They are either uncertain themselves, or based on uncertain information. Therefore, the target-response process of ATC must be modified so that sufficient information is passed between the connecting elements in the hierarchy to ensure the entire system does not exceed its maximum allowable failure probability, P_a, while optimizing the system in a decomposed manner. When the information shared between two elements is an uncertain design variable, only the point estimate of the uncertain variable, x_i, needs to be coordinated. For this study, x_i is defined both as a point estimate for an uncertain variable and as a deterministic variable. This is intentional as the goal of the decomposition of the uncertain variable into the point estimate and uncertain parameter is to allow a way for the optimization to treat uncertain variables in the same way that deterministic variables are treated. The same belief structure is referenced by the constraints in all elements. Thus, when the coordinated point estimates are equal, the coordinated uncertain variables will be exactly equal, with the same number of focal elements and associated upper and lower bounds.

When the shared information is a response quantity that depends on two or more uncertain variables and/or parameters, the target-response coordination process becomes more complicated. First, a joint belief structure is created for each response function in

the element ij using Eqs. (4.3) and (4.4), then the upper and lower bounds of the uncertain function are calculated in each joint focal element to obtain the corresponding response belief structure. While the BPA value for each joint focal element does not change the upper and lower bounds of the response function in each joint focal element can change. The calculation of the response bounds in each joint focal element and their matching with the corresponding target belief structure requires a large amount of computer memory, increasing the computational costs and finding an exact match between multi-level elements nearly impossible. This method proposes the use of a single characteristic number (CN) that is passed between the elements for a given target-response coordination. There are many ways of defining a CN, those explored here are the constraint bound, off-constraint bound and weighted mean values of the uncertain function.

Before proceeding, several terms need to be defined. The best way to do this is to detail the steps of the target-response process with uncertainty as shown in Figure 5.1. For a given element in the multilevel hierarchy, there is a vector of design variables, x_i, and perhaps one or more uncertain parameters, $\boldsymbol{P}_i$. Uncertain design variables are decomposed into point estimates and uncertain parameters. The belief structures of the uncertain variables and parameters are combined into a joint belief structure. Functions such as targets, responses, or constraints that depend on uncertain variables or parameters are calculated from the joint belief structure and the deterministic variables. The evaluation of these functions produces an interval for every focal element in the joint belief structure. For simplicity, this set of intervals will be referred to as the function's belief structure. The function belief structures are shown vertically to distinguish them

from the input belief structures of the uncertain variables and uncertain parameters. Each function produces a separate output belief structure for the same input joint belief structure and design variables. For simplicity, the Figures 5.1, 5.2, and 5.3 show the total range of the function's belief structure rather than the individual focal elements within that structure.

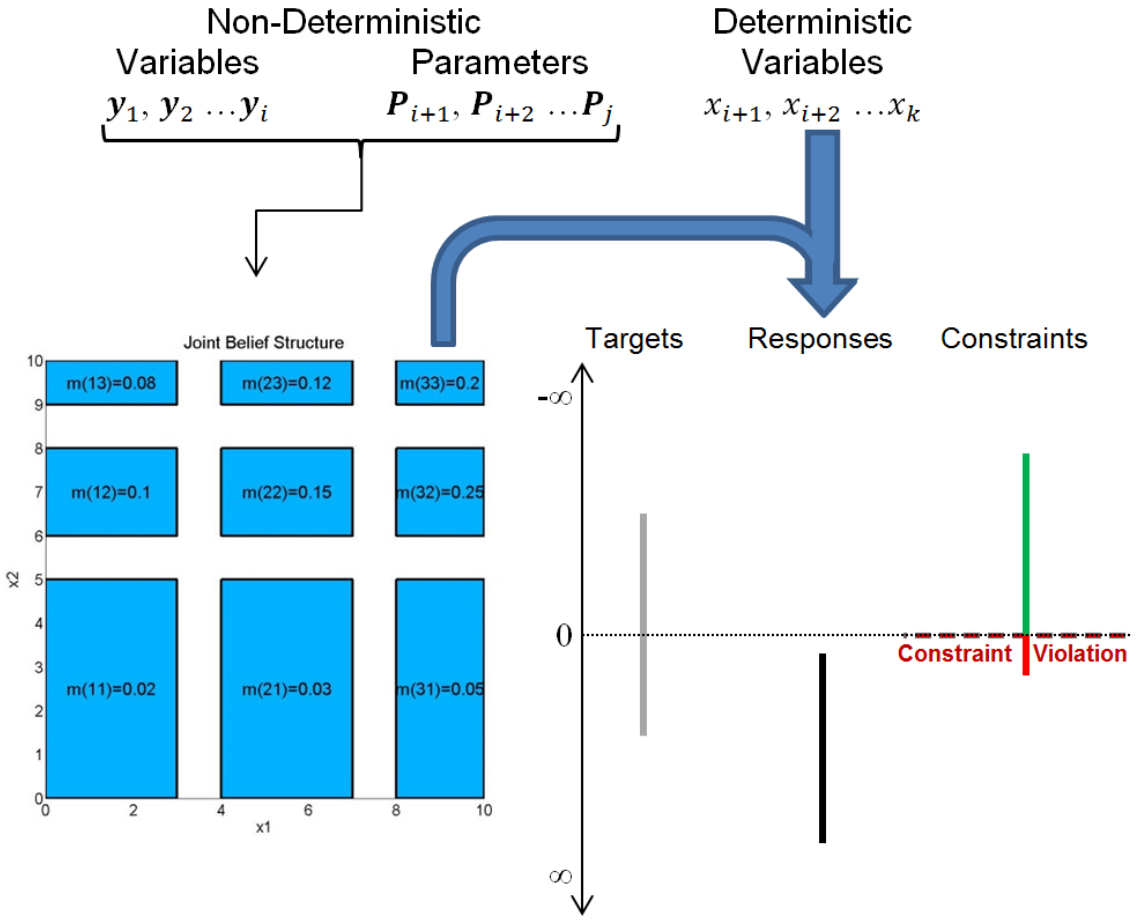

Figure 5.1 Diagram of the flow of information for EBMLDO

The thought experiment in the following chapters assumes that the target, response, and constraint functions are monotonic and that the gradients of all constraints

with respect to a given target or response have the same sign over the whole design space. This assumption means that the constraint values are linked to the target and response values. Thus, the constraint violation can be correlated to a target or response value for a given set of variables.

Consider the case where no failure is allowable, $P_a = 0$, and the target and response belief structures have differing ranges as shown in Figure 5.2. In this figure, the range of the uncertain target is shown in grey on the left for each set. Only the single number, represented by the solid circle, is passed between multilevel elements. The range of the response is shown next to the target. The additional range of the response is shown in red if it is below the line of constraint violation when the response is coordinated with the target and green if it produces a margin from failure. The constraint bound CN, shown in Figure 5.2 (a), matches the values closest to the constraint violation. In this case, there is a zero likelihood of constraint violation, but there is a chance for an overly conservative answer as shown by the green bar which extends farther away from the constraint violation than the target value. The off constraint bound CN, shown in Figure 5.2 (b), aligns the bound of the belief structures farthest from constraint violation. This method allows constraint violation in the response as the additional range of the response must violate the constraint. The weighted mean CN, shown in Figure 5.2 (c), aligns the function's weighted mean calculated as $WM = \sum_{i=1}^{nfe} \frac{f_i^l + f_i^u}{2} m(i)$ where f_i^l and f_i^u are the lower and upper bounds of focal element i of the target or response function f and nfe is the number of focal elements in f. This CN leads to a balance of violation and conservatism as long as the contributing response is balanced (the weighted mean is the average of the belief structure's absolute upper and lower bounds) and all equations that

the structure is used in are linear, otherwise it quickly strays to overly conservative or violation of constraint. Thus, the only method which ensures that the $P_a = 0$ constraint is met when the response is coordinated to the target is the constraint bound CN in Figure 5.2 (a).

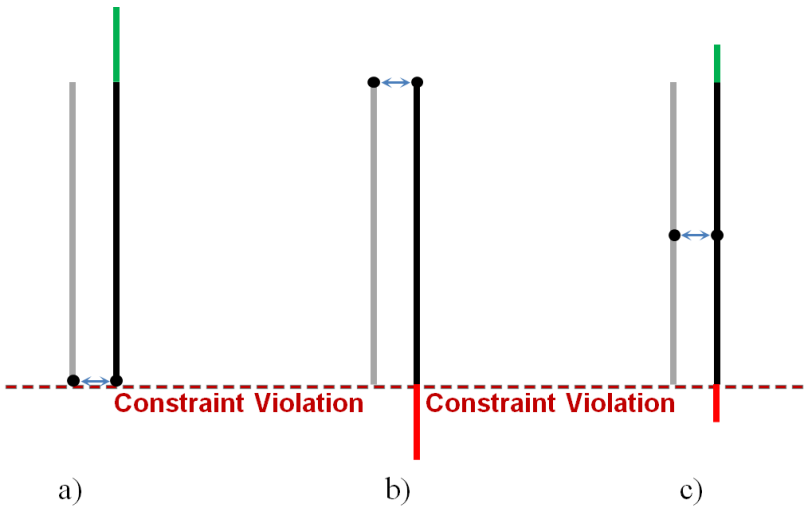

Figure 5.2 Target-response coordination for characteristic numbers with $P_a = 0$

a) Constraint bound characteristic number
b) Off-Constraint bound characteristic number
c) Weighted mean value characteristic number

When $P_a > 0$, there are slight differences in the application of the CN. Each element designs to the globally defined allowable probability of failure which allows a certain degree of failure. In Figure 5.3, the portions of the response shown in blue represent the allowable plausibility of failure. While these portions of the response violate constraints, they are less than P_a and, therefore, allowable. To ensure that P_a is met as closely as possible without violation, the passed value should be the value closest to constraint violation, which does not violate constraint as shown in Figure 5.3 (b). However, finding this value is computationally expensive as each focal element has to be

analyzed for compliance. Finding the constraint bound value, as shown in Figure 5.3 (a), is much easier as it only requires analysis of the bounds without analyzing compliance. This may lead to less than optimal solutions compared to the constraint value, but should not violate the constraints.

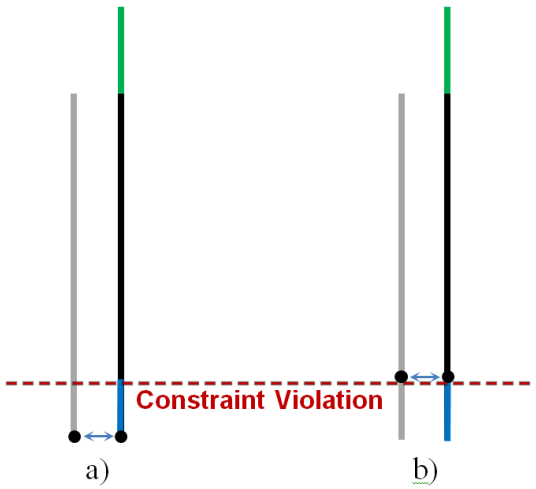

Figure 5.3 Target-response coordination for characteristic numbers with $P_a > 0$

a) Constraint bound characteristic number
b) Constraint value characteristic number

The three-beam, two-rod problem proposed by Allison et al. (2005) was used to determine the validity of each CN. The free body diagram of the problem is shown in Figure 5.4. It consists of three beams connected by two rods with all members having a circular cross section. The beam diameters, d_j for $j = 1 \ldots 3$, and rod diameters, $d_{r\,k}$ for $k = 1 \ldots 2$, are design variables, and all are considered uncertain for this exercise. The uncertainty is multiplicative in the form $\boldsymbol{y}_i = x_i \, \boldsymbol{P}_i$ with the initial uncertainty of ±1%. The exact belief structure used for this exercise is unimportant, because to achieve $P_a = 0$ the entire range of the variable has to satisfy the constraints; thus, only the upper and

lower bounds, +1% and -1% respectively, are needed. Constraints for the system are the maximum normal stress ≤ 127 MPa for each member, beam 1 maximum vertical deflection, $f_1 \leq 27mm$, and a maximum force transferred to the support of each beam, $F_{t\,j} \leq 400\ N$. The problem is divided into three elements as proposed by Tosserams et al. (2006). Element 1 optimizes beam 1 and rod 1, element 2 optimizes beam 2 and rod 2, and element 3 optimizes beam 3. The transferred pieces of information are the deflection of the beam, f_i, and the force passed to the structure above, F_i, which represent uncertain responses, but are functions of the uncertain variables. The targets from element 1 are calculated using the uncertain beam 1 and rod 1 diameters. The responses from element 2 are calculated using the uncertain beam 2 diameter. Similarly, the targets from element 2 are calculated from the uncertain beam 2 and rod 2 diameters. The responses from element 3 are calculated from the uncertain diameter of beam 3.

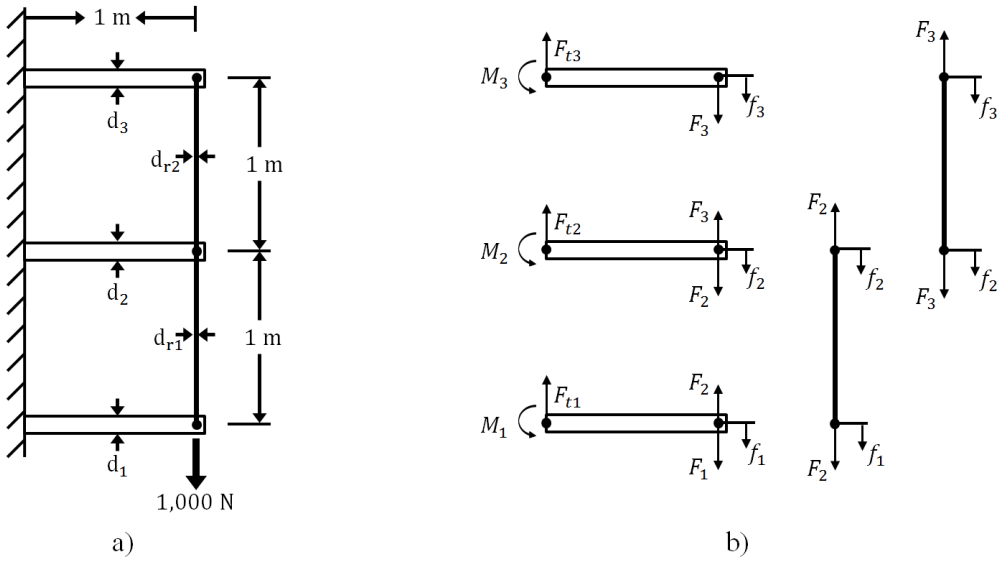

Figure 5.4 Structure used to validate characteristic numbers' target-response process

a) Structure with applied loading
b) Forces, moments, and deflections on each rod and beam

In this analysis, the constraints were used to solve for a viable solution with $P_a = 0$ then $P_a = 0.1$ to test both the $P_a = 0$ and $P_a > 0$ cases. This analysis is not intended to find the optimal design, merely a valid design point on the constraint boundary to judge the validity of each CN. The plausibility of failure was then tested using a simple finite element matrix with six nodes to ensure that the solution's plausibility of failure was, in fact, zero. This allowed the design points produced by using the different CNs to be tested for validity and compared to the correct solution.

The $P_a = 0$ cases were tested first. The analysis showed that the weighted mean CN caused constraint violation. The constraint and off-constraint bound CNs both produced valid results with the off-constraint bound weights being slightly higher when symmetric belief structure is used, but when asymmetric belief structures (+1/-2% and +2/-1%) were used, the constraint bound CN provided a better solution and better correlation to the actual values of the transferred information. The off-constraint bound CN yielded feasible but less than optimal results because, in this case, the target range was greater than the response range. As expected, the constraint bound CN produced more optimal results.

The analysis was repeated for $P_a = 0.1$ using the constraint bound CN only as it is both computationally inexpensive and guarantees that $Pl < P_a$. For this analysis, all uncertain variables use the same base belief structure shown in Figure 5.5 (a) for the initial analysis. This resulted in a plausibility of failure, $Pl = 0.0032$. Obviously, this is much less than the allowable plausibility of 0.1. This is due to the conservative nature of the constraint bound CN. To show this, the analysis was performed again using the belief structures where the most active focal element, the one closest to failure, was spaced

away from the other focal elements. For these belief structures, the weighted mean remained the same. These belief structures are shown in Figure 5.5 (b) and (c). For these belief structures, the plausibilities of failure were $Pl = 0.04$ and $Pl = 0.09$, respectively. This trend toward the allowable probability of failure is due to the lower interference from the other focal elements. It should be noted that the belief structure used in the final analysis is very near the range of uncertainty above which there is no feasible solution for this problem. This final analysis shows that this method will not violate constraint. The constraint bound value CN provides the lowest computational time while still ensuring no constraint violation.

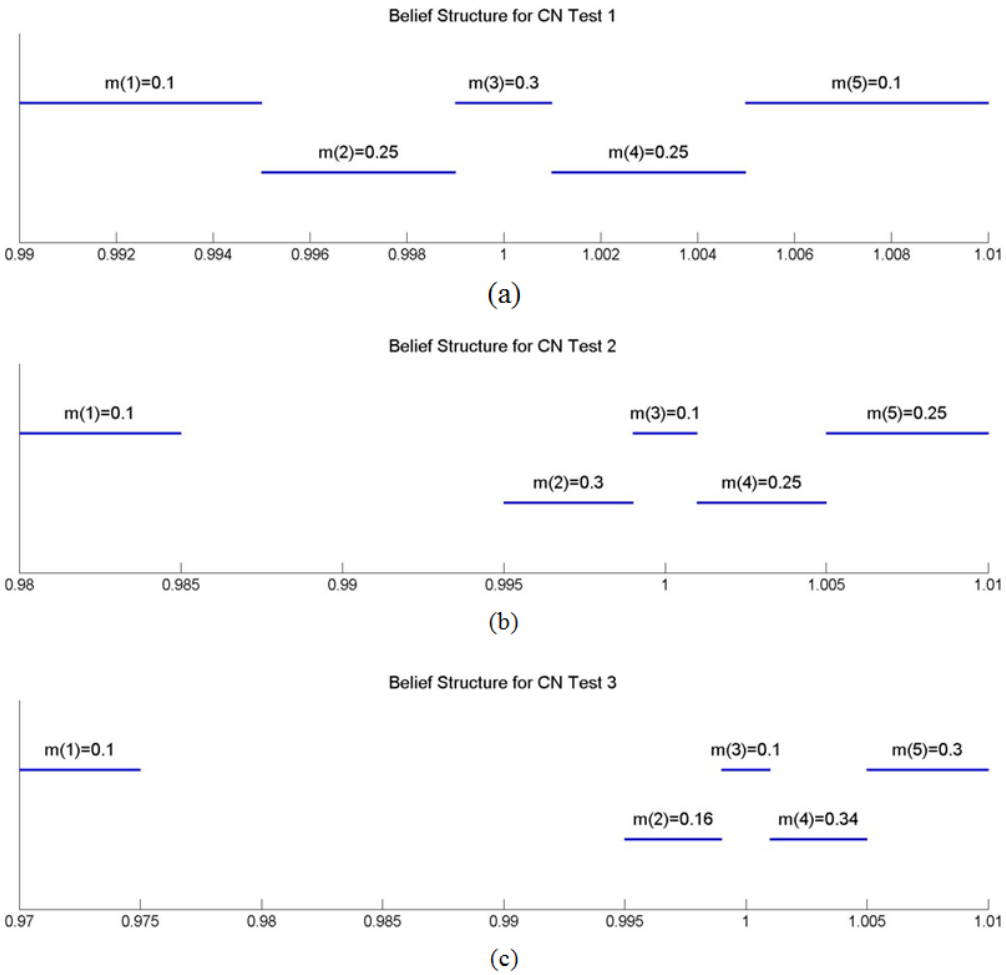

Figure 5.5 Belief structures used to test characteristic numbers for $P_a > 0$

(a) Belief structure with -1 / +1 % bounds
(b) Belief structure with -2 / +1 % bounds
(c) Belief structure with -3 / +1 % bounds

One of the disadvantages of the EBDO formulation is that it introduces complications in the optimization process. Due to the piecewise constant nature of plausibility, the gradient of the constraints is undefined over the entire domain regardless of the constraint. Thus, a zeroth order optimization method is needed. For this work, a genetic algorithm (GA) was chosen, though any such optimizer should work. A preliminary investigation showed that the decomposed multilevel process is only

convergent if legacy information is included in the initial GA population for the each inner loop. Thus, the previous best solution is inserted as one member of the larger initial population with the other members being random. This means that most of the time the previous best solution from the initial population is the previous best solution, but sometimes one of the random members is better. This allows a thorough examination of the design space while not restarting the optimization process in each iteration.

The use of a zeroth-order optimizer requires a change in the convergence criteria. While $\left\|c_{ij}^{n} - c_{ij}^{n-1}\right\| < \tau$ is satisfactory for gradient-based optimizers, with GA, this same condition could merely mean that the best solution from the last iteration is the best of the initial population and the new members introduced as a result of crossover and mutation operations are also inferior to the previous best solution. This can lead to premature convergence or a vastly uncoordinated result. Therefore, this work proposes the use of three convergence criteria: $\left\|c_{ij}^{n} - c_{ij}^{n-1}\right\| < \tau$, $f^{n} - f^{n-1} < \tau/10$, and $c_{ij}^{n} < \tau$, where f^{n} is the solution to the current iteration. The criterion $f^{n} - f^{n-1} < \tau/10$ is primarily used in double loop ATC configurations as the inner loop convergence criterion (Tosserams et al. 2006) and $c_{ij}^{n} < \tau$ is added to ensure a coordinated final solution.

CHAPTER VI

MULTILEVEL OPTIMIZATION WITH UNCERTAINTY

Formulation of Example Problems

The evidence-based multilevel design optimization (EBMLDO) framework presented in Chapter V was applied to two example problems to demonstrate the framework's application and performance. These problems were selected because they meet all criteria for decomposition and have low computational costs. The low costs are important because the addition of uncertainty to an optimization framework increases the computational costs significantly. All optimizations were performed using MATLAB®.

For determination of the upper and lower bounds of a response function in each joint focal element (for the plausibility of failure calculation), the gradient-based optimizer *fmincon* was used with the interior-point algorithm and the gradients determined using the forward finite difference method. Each element of the multilevel hierarchy was optimized using GA with an initial population of 30, a uniform creation function, a scattered crossover function with 0.8 crossover fraction, and two elite members passed to the next generation.

Problem 1

Problem 1 is the nondeterministic version of the two bar truss problem presented in Chapter 2. All three design variables, shown in Figure 2.3, are considered uncertain

using the same belief structure shown in Figure 6.1, which is multiplied by the point estimates expressed as $\boldsymbol{y}_i = z_i \boldsymbol{P}_i$, where the belief structure, $\boldsymbol{P}_i$, varies from 0.95 to 1.05. The belief structure used simulates tolerances of ±5% on the bars' areas and the truss height. This belief structure is symmetric about $y = 1$, so the point estimates are the weighted mean values.

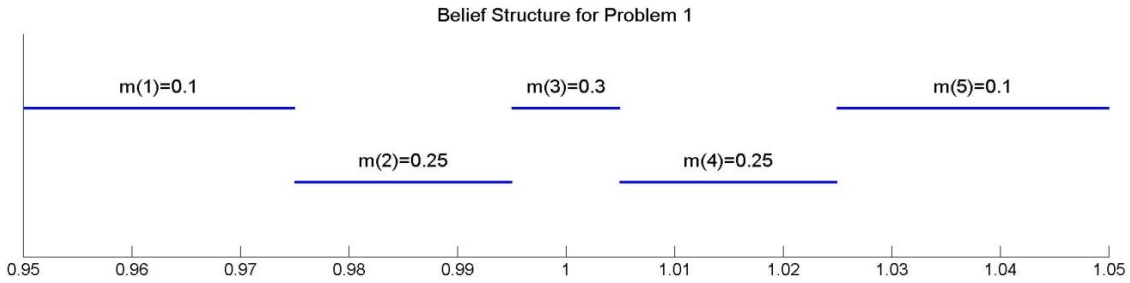

Figure 6.1 Belief structure used for Problem 1

The uncertainty quantification is implemented on the inequality constraint in each element. This implementation seeks to reduce the mean weight of the system rather than the uncertainty in the system as other formulations of EBDO (Bae et al 2004). The hierarchical decomposition of the problem with uncertainty is shown in Figure 6.2. This decomposition varies from the decomposition shown in Figure 2.4 in the formulation of the constraints; this one having nondeterministic constraints.

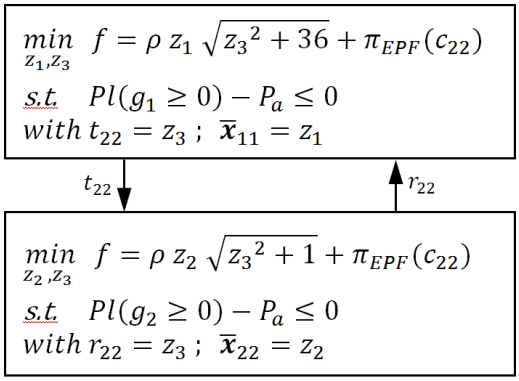

$$\pi_{EPF}(c_{22}) = \{\frac{\mu_{22}}{a_{22}}\left(e^{a_{22}\,(t_{22}-r_{22})} - 1\right) + \frac{\gamma_{22}}{b_{22}}\left(e^{b_{22}\,(r_{22}-t_{22})} - 1\right)\}$$

Figure 6.2 Hierarchical decomposition of Problem 1 in Chapter 2 with uncertainty

To gain a more thorough understanding of the effects of double-loop versus single-loop implementation of ATC and the effect EPF factors, this optimization problem was solved more than 300 times changing the loop form, the various EPF parameters ($\beta, a_0,$ and b_0), and the initial design point. A summary of these results is given below.

From both the single and double loop results, it was found that the initial design point must be feasible (all plausibility constraints must be satisfied). It was also observed that better results were achieved when the initial weights and multipliers are balanced ($a_0 = b_0$ and $\mu_0 = \gamma_0$) and either the initial weights, a_0 and b_0, or the updating factor, β, are closer to the upper bound while the other is closer to the lower bound of their recommended ranges. The recommended values of β are between 1 and 2. The initial multipliers, μ_0 and γ_0, are scaled as needed so that the penalty portion of the function can properly influence the overall objective function. The recommended values for initial weights, a_0 and b_0, are between 1 and 5. So for $a_0 = b_0 = 3$, a lower updating parameter of $\beta = 1.2$ is recommended.

The double-loop implementation of the problem took 58% longer per run (averaging 253 CPU minutes)[1] versus the single-loop average of 160 CPU minutes for $P_a = 0.2$. The double-loop strategy, however, was less likely to converge to a local minimum and was much less sensitive to changes in initial parameters, making it much more likely to find the global optimum with any given run.

The best solutions to the non-deterministic version of Problem 1 are summarized in Table 6.1 and compared with the deterministic optimum solutions using two different optimization methods (i.e., SQP and GA). The EBMLDO problem was optimized for P_a values of 0.2, 0.05, and 0.01. These results show that the designs that use evidence theory (ET) converge to larger system weights, as expected, but the optimum values would be hard to predict without this analysis. For instance, the truss height decreased for P_a values of 0.20 and 0.05, but the truss height for P_a = 0.01 was greater than the deterministic solution's height. There is also fair agreement between the AAO and the EPF solutions. However, in all the non-deterministic cases, the EPF+ET solutions are better than the AAO+ET solutions. This is believed to be mainly due to the fact that more runs were completed with EPF+ET, and the small, allowable difference between target and response allowing a marginal improvement. The inherent randomness of GA means that the larger the number of runs, the more likely one is to find a better optimum. As a result of adding uncertainty, both EBDO and EBMLDO require higher computational cost and time for finding the solution. This increase in costs has been observed with any optimization under uncertainty technique. The deterministic optimum converged with

[1] Microsoft Windows XP SP2; Processor Intel® Pentium® D CPU 3.00 GHz, 1.00 GB RAM

1,380 computations in 2 seconds using EPF and SQP. In contrast, it took the $P_a = 0.2$ EBDO solution 13 million computations in 3,837 seconds (64 minutes) to converge and the comparable EBMLDO solution over 47 million total optimization computations in 14,836 seconds (247 minutes). This represents a huge cost for implementing ET. The increase in time and computations between the EPF and AAO formulations reflects the simplicity of the original problem. The original problem is only slightly more complex than each element of the decomposed problem. Decomposed optimization only shows advantages when the original problem is much more complex than the decomposed elements.

Table 6.1 Summary of results of Problem 1.

Approach	P_a	z_3: t_{22}	z_3: r_{22}	z_1	z_2	f^*	c_{22}	GAcost	Time (s)
Deterministic Solutions									
EPF+SQP	-	2.4495	2.4495	0.003780	0.009258	3,747.7	0.000472	-	3
EPF+GA	-	2.2910	2.2908	0.004006	0.009347	3,755.8	0.000263	76,814	36
Non-Deterministic Solutions									
AAO+ET	0.20	2.5745	-	0.003798	0.009456	3,895.1	-	3,150	3,837
EPF+ET	0.20	2.4061	2.4056	0.004024	0.009546	3,892.5	0.000529	23,460	14,836
AAO+ET	0.05	2.5829	-	0.003880	0.009712	3,996.8	-	3,150	3,848
EPF+ET	0.05	2.3745	2.3739	0.004168	0.009806	3,990.5	0.000595	31,740	20,642
AAO+ET	0.01	2.4273	-	0.004115	0.009801	4,005.7	-	3,150	3,835
EPF+ET	0.01	2.5212	2.5211	0.003967	0.009762	4,000.9	0.000098	12,420	7,597

Comparing the optimum objective function of the all-at-once, EBDO, solutions to the decomposed results, EBMLDO, reveals very similar values for the objective function but dissimilar values for system height. This is achieved by differing values of the bar cross sectional areas. In the deterministic formulation of this problem the comparison of the objective function and the system height is defined by a fourth order polynomial with a single minimum. The solution with uncertainty included is also defined by a fourth

order polynomial but with two global minima. While the AAO and decomposed solutions differ in each case this is merely because each is finding a different global minima. While each solution converged to each minima, the best solution for each method was a different global minima (due to the relatively loose tolerance and randomness of genetic algorithm).

Problem 2

Problem 2 is a nonlinear, seven-variable, optimization problem formulated as

$$\begin{aligned} \min_{x_i} f &= {x_1}^2 + {x_2}^2 \\ s.t.\quad g_1 &= {x_3}^{-2} + {x_4}^2 - {x_5}^2 \leq 0 \\ g_2 &= {x_5}^2 + {x_6}^{-2} - {x_7}^2 \leq 0 \\ h_1 &= {x_3}^2 + {x_4}^{-2} + {x_5}^2 - {x_1}^2 = 0 \\ h_2 &= {x_5}^2 + {x_6}^2 + {x_7}^2 - {x_2}^2 = 0 \\ x_1, x_2, \ldots, x_7 &\geq 0 \end{aligned} \tag{6.1}$$

where at the deterministic point of optimum $\boldsymbol{x}^* = [2.149,\ 2.076,\ 1.316,\ 0.760,\ 1.075,\ 1.000,\ 1.463]$, $f^* = 8.93$ and all constraints are active. The problem is decomposed into the two-element hierarchy proposed by Tosserams (2004) as shown in Figure 6.3 for the EPF formulation.

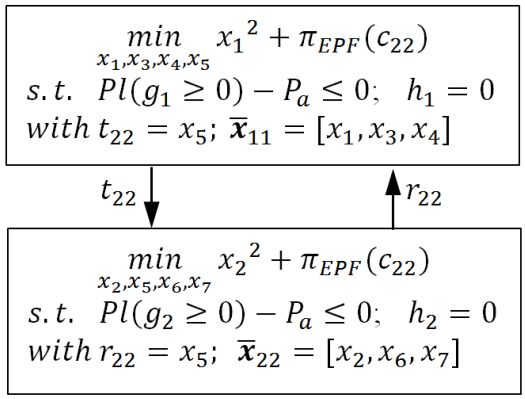

$$\pi_{EPF}(c_{22}) = \{\frac{\mu_{22}}{a_{22}}\left(e^{a_{22}(t_{22}-r_{22})} - 1\right) + \frac{\gamma_{22}}{b_{22}}\left(e^{b_{22}(r_{22}-t_{22})} - 1\right)\}$$

Figure 6.3 Hierarchical decomposition of Problem 2

The variables x_3, x_5, and x_7 are considered uncertain. All three uncertain variables use the same belief structure shown in Figure 6.4. The uncertainty is added to the point estimate of each variable with the absolute upper and lower bounds expressed as $\boldsymbol{y}_i = x_i \pm 0.5$. Because the belief structure is symmetric around zero, the point estimate is the same as the weighted mean. Only the point estimate value of the shared variable, x_5, is passed between the two elements. The uncertainty is only considered in the inequality constraints and the point estimates are used to determine compliance with the equality constraints. The side constraints are modified to account for uncertainty, and enforced on the point estimate.

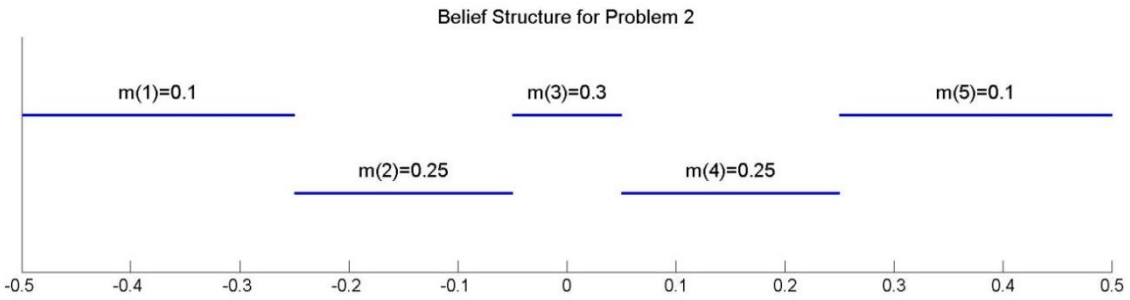

Figure 6.4 Belief structure used for problem 2

To simplify the problem and find the effect of the equality constraints, the equality constraints were used to express x_1 and x_2 as functions of the other variables. These were substituted into the original problem to produce a five variable, non-linear optimization problem:

$$\begin{aligned} \min_{y,z_1,z_2} \; & f = [\, {x_3}^2 + {x_4}^{-2} + {x_5}^2 \,]^2 + [\, {x_5}^2 + {x_6}^2 + {x_7}^2 \,]^2 \\ s.t. \quad & g_1 = {x_3}^{-2} + {x_4}^2 - {x_5}^2 \le 0 \\ & g_2 = {x_5}^2 + {x_6}^{-2} - {x_7}^2 \le 0 \\ & x_3 \,, x_2, \ldots, x_7 \ge 0 \end{aligned} \tag{6.2}$$

The original numbering scheme is retained for ease of recognition, but x_1 and x_2 have been eliminated.

Only the double-loop strategy was used for this problem. The results are presented in Table 6.2. These solutions all used $P_a = 0.2$. The increase in computational time is once again observed to be very high, but the costs are nearly 5 times less for the case with no equality constraints. This is probably due to the randomness inside of GA

whose generated points are unlikely to satisfy the equality constraint. Therefore, it is recommended that equality constraints be eliminated, if possible.

Table 6.2 Summary of results from problem 2.

Solution	$x_5: t_{22}$	$x_5: r_{22}$	f^*	c_{22}	$a_0 = b_0$	GAcost	Time (s)
EPF+GA[a]	1.0745	1.0745	8.928	1.35E-7	-	9,740	5
EPF+ET full	1.3760	1.3350	13.248	0.04096	5	234,384	164,324
EPF+ET no equality	1.2497	1.2561	12.615	0.06450	5	55,200	33,933

[a] Deterministic optimum solution.

On the Effect of Belief Structure

Once it was shown that the EBMLDO approach was able to solve an optimization problem under epistemic uncertainty, it was used to solve the two bar truss problem from above with various belief structures. The goal of this study was to determine exactly how the belief structure affects the final solution in hopes of being able to replace expensive belief structures (those with large numbers of focal elements) with less expensive belief structures. Each focal element eliminated would result in a reduction in the time needed to calculate the plausibility of failure. Since this calculation is performed many times throughout the optimization, this can result in a significant time savings. The belief structures tested are shown in Figure 6.5.

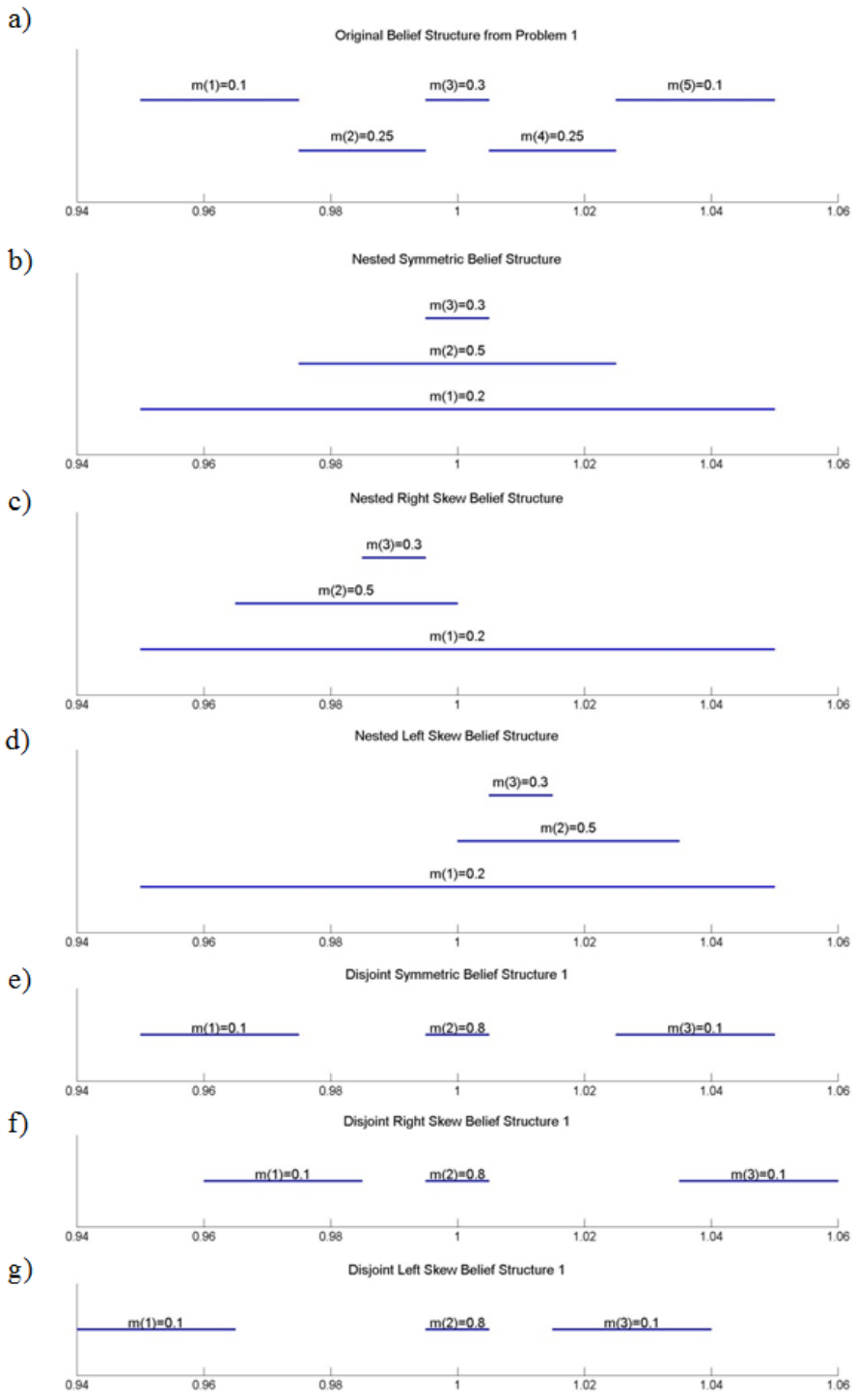

Figure 6.5 Belief structures tested to determine their effect

a) Original Belief Structure in Problem 1 b) Symmetric, Nested Belief Structure
c) Right Skewed, Nested Belief Structure d) Left skewed, Nested Belief Structure
e) Symmetric, Disjoint Belief Structure 1 f) Right skewed, Disjoint Belief Structure 1
g) Left Skewed, Disjoint Belief Structure 1

Nested and disjoint belief structures were each tested with a right skewed, a left skewed, and a symmetric belief structure. All the belief structures used three focal elements and tried to mimic the original belief structure from Problem 1 as closely as possible while still meeting its designated criteria. For all these optimizations a maximum allowable probability of $P_a = 0.2$ was used.

The optimum solutions are shown in Table 6.3. For these results, the right skewed belief structure produced a higher objective function than the symmetric belief structure, while the left skew produced an objective function lower than the symmetric result. This does not match the expected results. For a right skewed belief structure, the "outliers" are located on the higher (right) side of the belief structure. Since the failure side is the lower (left) side, one would expect the right skewed result to be lower. This is believed to be due to the construction of the belief structure in that the weighted mean of the skewed belief structures is not 1. Looking just at the symmetric case, the results of the nested belief structure are significantly higher than those for the original belief structure, and the results of the disjoint belief structures are significantly lower than the other two. This was unexpected as each new belief structure was designed to be as similar to the original as possible. Note the dissimilarity in different measures of computational cost between the original belief structure's results and the nested symmetric belief structure's results. While the time and the total number of optimization function calls used to calculate the plausibility of failure (defined in Tables 6.3, 6.4, 6.5 and 6.6 as CompCost) remain nearly the same, the total number of times that the genetic algorithm evaluated the objective function and constraints (defined in Tables 6.3, 6.4, 6.5 and 6.6 as GAcost) increases

significantly. This is because different weights and updating factors are used, decreasing the convergence speed of EPF.

Table 6.3 Raw optimum solutions for various belief structures

Belief Structure	z_3: t_{22}	z_1	z_2	f^*	c_{22}	GAcost	CompCost	Time (s)
Original Belief Structure (Figure 6.5 a)								
Original	2.4061	0.004024	0.009546	3,892.5	0.000530	23,460	47,844,254	14,836
Nested Belief Structures (Figure 6.5 b, c, & d)								
Symmetric	2.5027	0.003977	0.009557	3,950.8	0.003571	59,340	42,139,486	13,106
Right Skew	2.2524	0.004407	0.009838	4,015.4	0.000098	64,500	45,341,579	14,277
Left Skew	2.1844	0.004370	0.009571	3,894.4	0.000798	98,040	69,245,164	20,708
Disjoint Belief Structures $m(2) = 0.8$ (Figure 6.5 e, f, & g)								
Symmetric	2.3444	0.003962	0.009431	3,791.4	0.000069	64,500	44,495,915	13,337
Right Skew	2.2427	0.004119	0.009480	3,796.0	0.004599	49,020	34,286,286	10,514
Left Skew	2.4199	0.003855	0.009348	3,779.8	0.000956	56,760	39,251,007	12,345
Disjoint Belief Structures $m(2) = 0.6$ (Same form as Figure 6.5 e, f, & g)								
Symmetric	2.4098	0.004028	0.009407	3,868.6	0.001795	103,200	72,504,341	23,139
Right Skew	2.5313	0.003896	0.009345	3,886.4	0.000763	180,600	126,443,030	43,956
Left Skew	2.5131	0.003849	0.009332	3,848.0	0.002951	126,420	88,018,548	28,423

When creating the right and left skewed belief structures, one of the focal elements was chosen to retain its upper and lower bounds. This means that, in order to obtain a right or left skew, the upper and lower bounds of the other two focal elements were moved. This resulted in belief structures where the weighted mean was not the point estimate for that belief structure. To gain a better understanding of these results, they were adjusted so that the weighted mean is the point estimate these results are shown in Table 6.4.

These results show the expected pattern between the symmetric, right skewed, and left skewed belief structures. This shows that it was the construction of the belief structures that caused the unexpected shifts above. The disjoint belief structures with $m(2) = 0.6$ result in an increase in the optimum objective function almost up to the

original optimum. This increase was expected as increasing the BPA of focal elements on the failure side of the belief structure should result in a more conservative answer. Each group from these results is much more clustered than those above. This means there is greater similarity between those in each group when the weighted mean is used as the point estimate. The reason for this is explained below.

Table 6.4 Solutions with weighted mean as point estimate for various belief structures

Belief Structure	z_3: t_{22}	z_1	z_2	f^*	c_{22}	GAcost	CompCost	Time (s)
Original Belief Structure								
Original	2.4061	0.004024	0.009546	3,892.5	0.000530	23,460	47,844,254	14,836
Nested Belief Structures								
Symmetric	2.5027	0.003977	0.009557	3,950.8	0.003571	59,340	42,139,486	13,106
Right Skew	2.2258	0.004355	0.009722	3,946.9	0.000097	64,500	45,341,579	14,277
Left Skew	2.2102	0.004422	0.009684	3,960.8	0.000807	98,040	69,245,164	20,708
Disjoint Belief Structures $m(2) = 0.8$								
Symmetric	2.3444	0.003962	0.009431	3,791.4	0.000069	64,500	44,495,915	13,337
Right Skew	2.2383	0.004111	0.009461	3,785.0	0.004581	49,020	34,286,286	10,514
Left Skew	2.4247	0.003863	0.009397	3,791.1	0.000958	56,760	39,251,007	12,345
Disjoint Belief Structures $m(2) = 0.6$								
Symmetric	2.4098	0.004028	0.009407	3,868.6	0.001795	103,200	72,504,341	23,139
Right Skew	2.5204	0.003880	0.009308	3,862.9	0.000760	180,600	126,443,030	43,956
Left Skew	2.5231	0.003864	0.009369	3,871.2	0.002963	126,420	88,018,548	28,423

Replicating Results with Different Belief Structures

From the results collected above, it appears that the most important feature of the belief structure is the cumulative plausibility function (CPF) from the failure side. The cumulative plausibility for any given point in the belief structure is the sum of all the BPAs of the focal elements to one side of that point including the BPA of any focal element the point lies in. There is a much sharper rise in the CPF among the nested belief structure than the original, and the disjoint CPF with $m(2) = 0.8$ is missing the second

rise that is present in the original CPF as shown in Figure 6.6. This is believed to be driving the nested results to be higher than the original and the disjoint results lower.

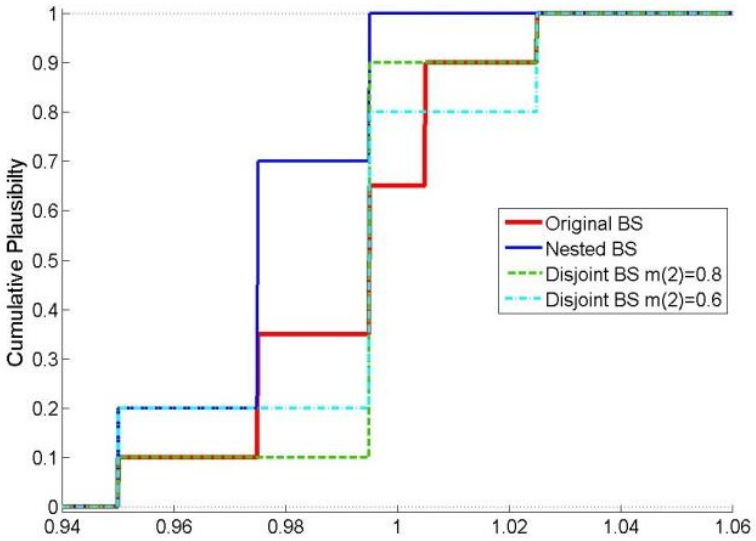

Figure 6.6 Comparison of the cumulative plausibility functions for tested belief structures

Because the cumulative plausibility just measures plausibility and not belief, one can create an infinite number of belief structures with the same CPF. It is important to note that this works only when the side of the belief structure that contributes to failure is known. In Problem 1 above, the failure side is known for the rod cross sectional areas (z_1 and z_2), as a smaller area gives a higher stress and is closer to failure. Unfortunately the side that contributes to failure is not always clear. For instance variable x_5 from problem 2 may cause failure by either increasing or decreasing. In the case of "black box" analyses, the effect of a variable may be unknown.

To test if the CPF was the only factor affecting the optimum solution, a new, nested belief structure, shown in Figure 6.7, with five focal elements was created to replace the belief structure used for the rods' cross sectional areas (z_1 and z_2) in Problem 1. Each focal element of this belief structure has the same lower bound as the corresponding focal element in the original belief structure, and all the focal elements in this belief structure have the same upper bound, 1.05, which is the same upper bound as the original belief structure. The new belief structure was applied only to the rods' cross sectional areas. The original belief structure was applied to the truss height. The results of this optimum are compared to the original results in Table 6.5.

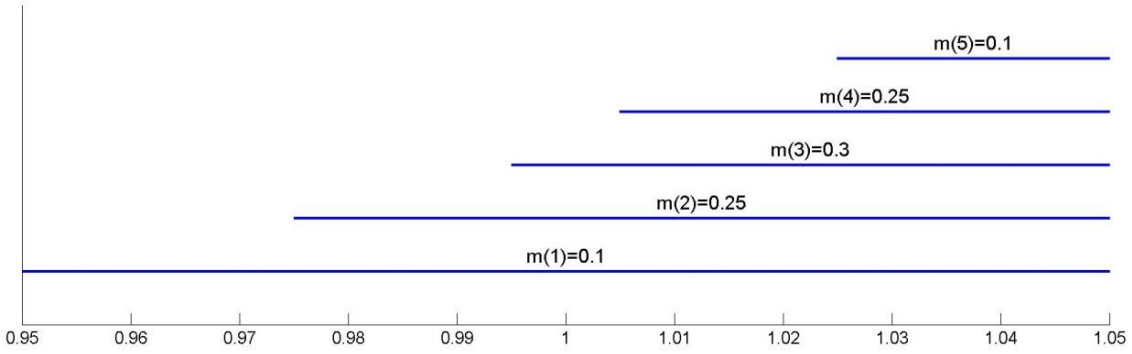

Figure 6.7 The belief structure with the same cumulative plausibility structure from the left side as the original belief structure from problem 1.

Table 6.5 Results from belief structures with same Cumulative Plausibility Structure

Belief Structure	z_3: t_{22}	z_1	z_2	f^*	c_{22}	GAcost	CompCost	Time (s)
Original	2.4061	0.004024	0.009546	3,892.5	0.0005296	23,460	47,844,254	14,836
New	2.4200	0.004003	0.009533	3,892.2	0.0020922	67,080	132,723,699	39,762

These results are nearly identical to the original results. This shows that the CPF drives the optimum point rather than the exact belief structure. Because of this, it is concluded that the weighted mean point estimate results from the last section matched each other better because their CPFs were more similar than those that did not use weighted mean point estimate. While there is a large difference in computational cost between these results, this is believed to be due to the weights and updating parameter used in the EPF formulation because of the very similar GAcost/Time. In fact if an average is taken over the 50 runs with each belief structure, the original belief structure took $1.608\ \mathrm{GAcost/s}$ while the new belief structure took $1.604\ \mathrm{GAcost/s}$. If the belief structure were the cause of the computational cost increase, one would expect a significant decrease in this statistic.

Decreasing Costs through Manipulation of Belief Structures

The next goal of this research was to reduce the computational costs while maintaining the same results by manipulating the belief structure. These attempts will focus on two variables to improve the efficiency of the system: the range of each focal element, and the number of focal elements. Because calculation of the plausibility of failure requires optimization operations to find the maximum and minimum value of the evaluated function in each focal element, it seems reasonable that reducing the uncertainty space would increase the speed and reduce the number of function calls required to solve the plausibility. The reduction in the number of focal elements reduces the number of optimization operations that need to be performed. The problem with reducing the number of focal elements is that it degrades the quality of the plausibility calculation. Thus, the eliminated focal elements need to be the ones of the least influence

over the final answer. This is achieved by eliminating the focal elements farthest from the failure side, once again assuming that the failure side of the optimization is known.

As shown in the section above, the same results can be achieved with a different belief structure as long as the CPF from the failure side remains the same. This can be achieved by moving the bound of a focal element that is away from the failure side. Since the goal is to reduce the range of each focal element, the range is set to the arbitrary small value of 0.001 as shown in Figure 6.8. Next the two focal elements farthest away from the failure side, focal elements 4 and 5, are eliminated and their BPAs are added to focal element 3, the closest remaining focal element to them as shown in Figure 6.8.

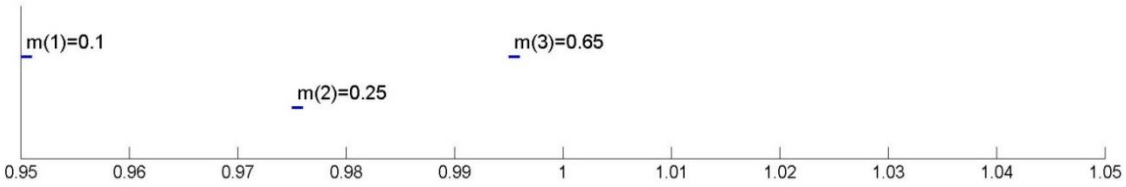

Figure 6.8 Belief structure which reduces costs while giving the same optimal point

The results in Table 6.6 show that the same optimum objective function value is achieved with the truncated belief structure as with the original belief structure. Hence, this truncated belief structure is functionally the same as the original belief structure, but can lead to less computational costs. While the number of optimization operations and the total time of the optimization are reduced, a greater measure of the efficiency of this belief structure is the large increase in the number of main optimization function evaluations (GAcost) per second, and the significant reduction in the number of constraint optimization function calls required to evaluate the constraints of the main function

(CompCost / GAcost). The improvement in these cost metrics is significant, because the cost reduction is even greater than that observed with the other belief structures with three focal elements tested above. These belief structures had about 4.6 GAcost/s and about 680 CompCost/GAcost, for an average increase of 22% in GAcost/s and 20% decrease in CompCost/GAcost. The observed increased efficiency suggests that the additional savings are due to the reduction in the focal elements' range, which allows the implementation of a cost reduction measure without eliminating focal elements. The focal element range can be reduced if the constraint is monotonic and the failure side is known regardless of the problem or which subset of the focal elements contributes to plausibility of a constraint failure.

Table 6.6 Results of belief structure in Figure 6.8 showing reduced cost metrics

Belief Structure	$z_3: t_{22}$	z_1	z_2	f^*	c_{22}
Original	2.4061	0.004024	0.009546	3,892.5	0.0005296
Same CPS	2.4200	0.004003	0.009533	3,892.2	0.0020922
Reduced Cost	2.4524	0.003958	0.009522	3,892.0	0.0002896
Belief Structure	**GAcost**	**$\frac{\text{GAcost}}{\text{s}}$**	**CompCost**	**$\frac{\text{CompCost}}{\text{GAcost}}$**	**Time (s)**
Original	23,460	1.581	47,844,254	2,039.4	14,836
Same CPS	67,080	1.687	132,723,699	1,978.6	39,762
Reduced Cost	49,020	5.634	26,316,983	536.9	8,701

These reveal how the belief structure can affect the optimization solution, but they also display an effective method for the integration of multilevel optimization and uncertainty quantification using evidence theory.

CHAPTER VII

MULTILEVEL OPTIMIZATION OF A TRANSPORT AIRCRAFT WING

The multilevel optimization framework is suitable for complex engineering systems that can be decomposed into smaller analysis and optimization sub-problems. The design problem considered in this chapter focuses on the material-product optimization of a transport aircraft wing (TAW) without consideration of the underlying uncertainties. The original problem considered the shape and sizing optimization of the wing for an aircraft similar to a Boeing 767 (Garcelon et al. 1999, Venter and Sobieski 2004, 2006). The TAW model is assumed to have sandwich composite skin panels with honeycomb core and fiber-reinforced polymer composite face sheets. In addition to the continuous reinforcing fibers, the vinyl ester matrix is enhanced using carbon nanofibers. In a recent study, DorMohammadi and Rais-Rohani (2014) developed a multilevel framework for the coupled material-product systems and demonstrated its application on the design of a rectangular composite sandwich plate with nano-reinforcements. Here, the wing structure will be optimized from the nano-reinforcements in the enhanced matrix and the sandwich wing panels to the wing's overall structure while holding the shape and applied loads fixed. While vinyl ester is not a preferred matrix material for an aircraft's primary structure, it is used here to maintain consistency with past research.

The use of advanced composites in aircraft structures leads to a large number of design variables to optimize under multiple failure modes. The design variables typically

include the thickness and angle of each ply along with core thickness, honeycomb cell size, and foil thickness. Within the face sheet material, the elastic properties and volume fraction of the continuous fibers and the carbon nanofibers control the stiffness of each ply. All of these variables combined lead to a large design optimization problem.

All wings have stiffness requirements, which are often introduced in an optimization problem as constraints on wing tip deflection, twist angle, and/or vibration frequencies. The use of sandwich design introduces failure modes such as shear crimping, face sheet dimpling, and face sheet wrinkling (Bruhn 1973). The wing structure with sandwich panels must be able to withstand all these failure modes while resisting fatigue and damage under normal operating conditions. All these failure modes require analyses that are sometimes quite computationally expensive. By isolating these analyses in several simpler problems the computational costs can be reduced, as discussed later in this chapter.

The TAW problem is decomposed into a three level hierarchy: the wing problem at the top level optimizes the wing's total weight subject to excessive deflections, the sandwich panel problem in the middle level optimizes the weight of the panel subject to failures of the skin, and the nano-enhanced matrix problem at the bottom level optimizes the polymer matrix for the face sheet laminate. As shown in Figures 7.1 and 7.2, the wing structural optimization is the system level problem. This wing is divided into two panel groups. Each group is optimized using its own multilevel optimization with two levels. In the original sandwich plate formulation (DorMohammadi and Rais-Rohani 2014), the sandwich plate was decomposed into three levels, but a two level formulation is used here to allow the use of first ply failure criterion which is expected to be a dominant

mode for the lower wing skin that operates mostly under tension. The macro-level structural/material problem optimizes each sandwich panel's composite laminate. The micro-level material problem optimizes the properties of the matrix through the use of carbon nanofibers. Each of these problems is more thoroughly explained in the following sections.

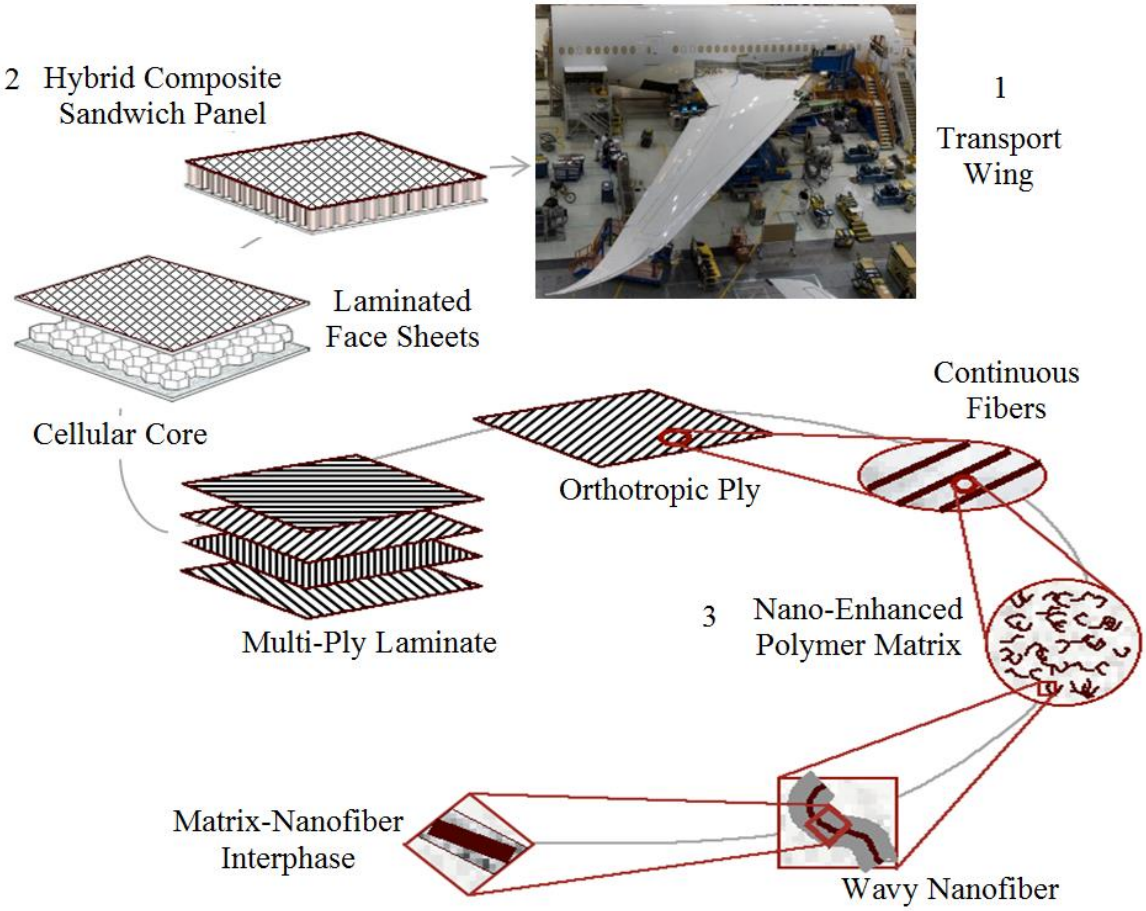

Figure 7.1 The multiple levels optimized in the transport aircraft wing problem.

Figure is modified from DorMohammadi and Rais-Rohani (2014). Wing photo reproduced with the permission of Air Canada.

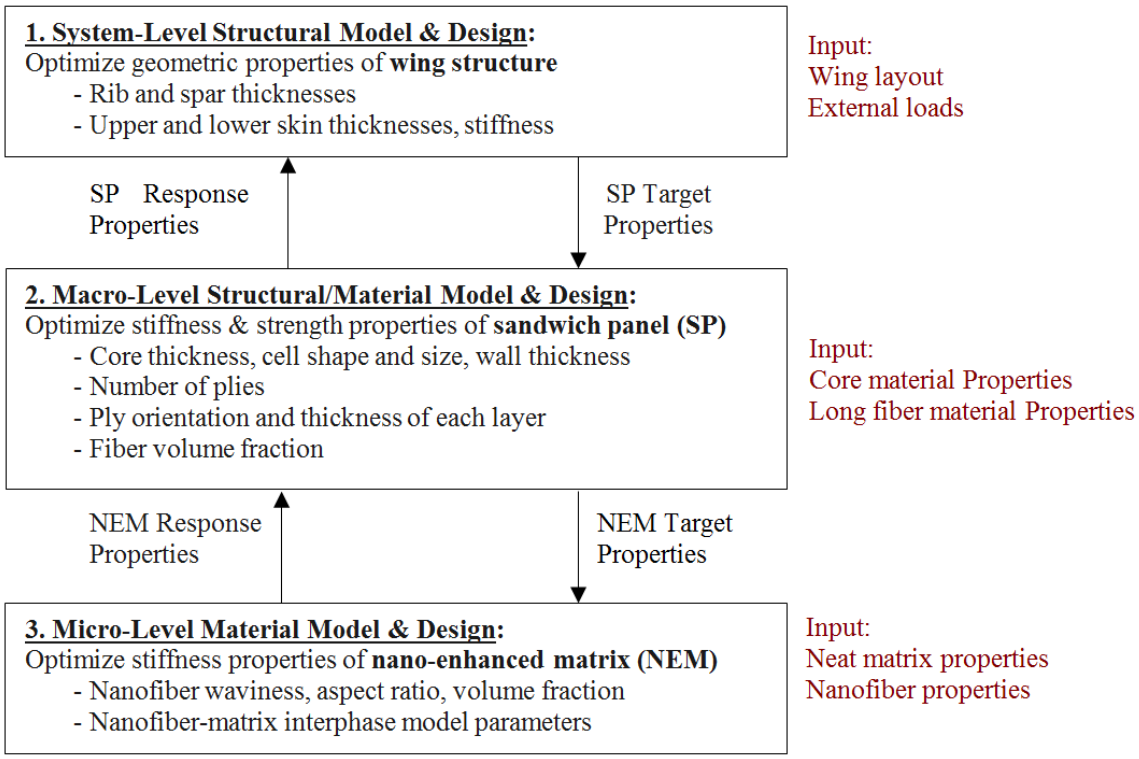

Figure 7.2 The decomposed framework showing the three levels of the transport aircraft wing problem, the corresponding inputs, and the variables

For this formulation, the wing was divided into two panel groups and two spar/rib groups. The panels and the rib/spar groups were divided at rib number 5 into separate inboard and outboard groups. Therefore the general hierarchy from Figure 7.2 becomes the problem specific hierarchy in Figure 7.3. For clarity, Elements 22 and 23 in Figure 7.3 correspond to Element 2 in Figure 7.2. Similarly, Elements 34 and 35 in Figure 7.3 correspond to Element 3 in Figure 7.2.

Both the upper and lower wing skins in each group are identical. Each wing skin panel group has 21 design variables and the wing has 4 design variables for a total of 46 design variables. For the decomposed formulation, 12 decision variables must be added,

eight in Element 11 to act as the targets for Elements 22 and 23 and two each in Elements 22 and 23 to act as the targets for Elements 34 and 35.

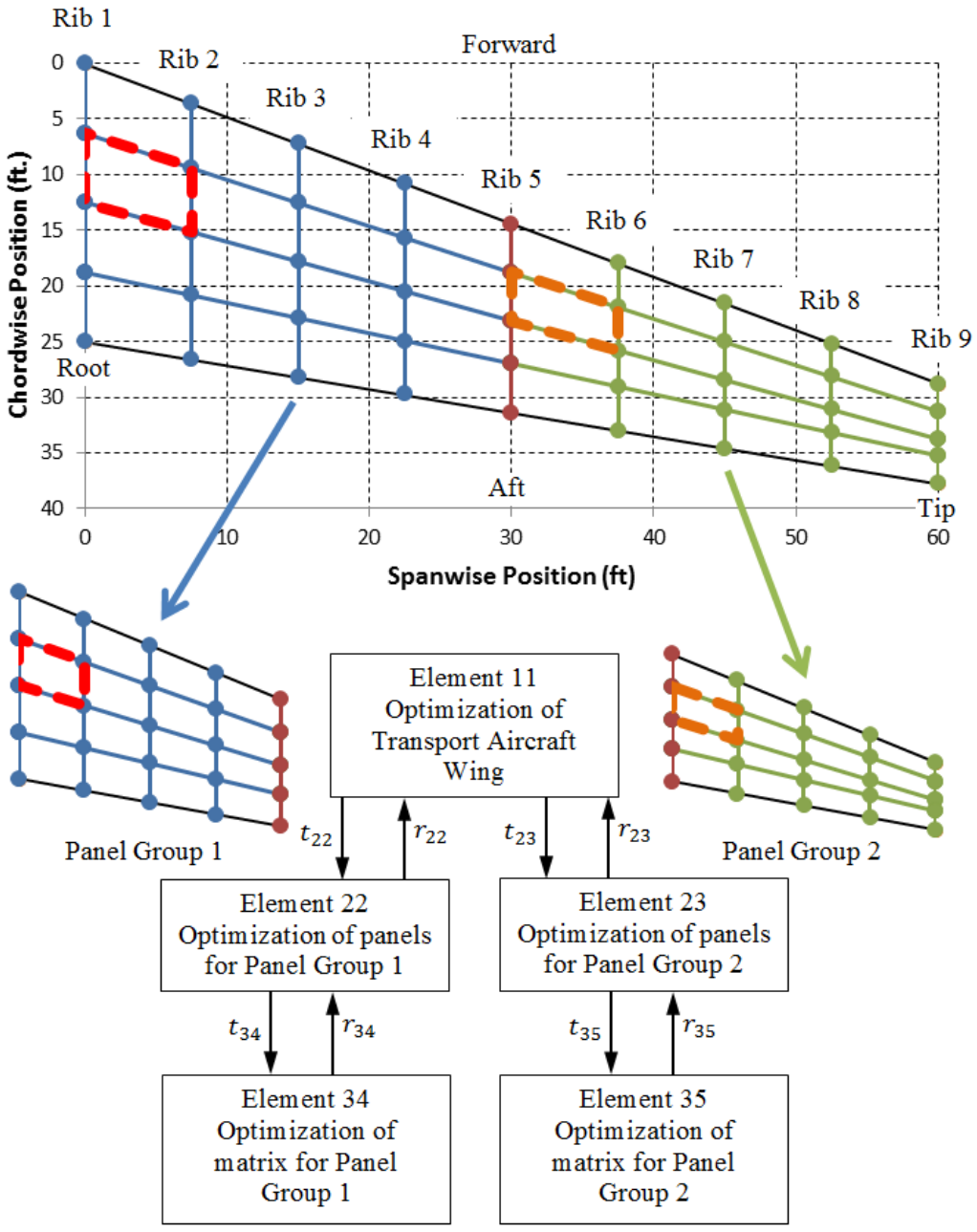

Figure 7.3 Two panel group decomposition of the Transport Aircraft Wing Problem

The critical panels are outlined in red and orange dashed lines for panel groups 1 and 2, respectively.

Element 11: System-Level Structural Model and Design

The top level problem (Element 11) optimizes the wing members' dimensions and the skin stiffness to minimize the wing's weight. For this problem, the spars and ribs are assumed to be only webs connecting the wing skins. There are constraints on the maximum compressive and tensile stresses in the spars and the ribs and on the maximum tip deflection and maximum tip twist. In the original problem, all the members are made of 6061 aluminum alloy with the wing skins being a sandwich of aluminum face sheets and Divinycell F40 foam core. In this formulation, the spars and ribs remain 6061 aluminum, but the skins are replaced with a carbon fiber sandwich composite with 2024 aluminum honeycomb as the core material. Although not directly modeled here, it is assumed that there is a proper barrier in the contact surfaces between the aluminum and carbon components to avoid galvanic corrosion. This skin material is the same as that used in the sandwich plate optimization problem (DorMohammadi and Rais-Rohani 2014); further details appear in the Level 2 description below. The combination of aluminum substructure with carbon fiber outer structure has been used in industry before. The Airbus A400M military transport and the Bombardier CS100, CS300, and CS500 commercial airliners feature carbon fiber reinforced skins and spars with aluminum ribs. The example here is different in using aluminum for the spars as well as the ribs.

The finite element (FE) model used for the top-level optimization problem is shown in Figure 7.4. Analyzed using MSC Nastran 2013.1 Student Edition, the model uses 72 membrane elements to model the three spar webs, eight rib webs and two skins. The root rib is not modeled and each node that would have been on that rib is held fixed against translation and rotation along all axes resulting in a clamped boundary condition.

Only the wing box is modeled using CQUAD4 elements, 2D quadrilateral membrane elements, denoted in Figure 7.4 by the light blue cross members bounded by the thick blue lines which outline each element. Loads are transferred from the leading and trailing edges of the wing by "rigid" RBE3 elements denoted by the red lines in Figure 7.4. Each skin panel is supported by two spars and two ribs giving a total of 32 skin panels.

Any number of these panels could be optimized using the full multilevel model or they could be grouped in any configuration to reduce the number of computations. For each group of panels, the variables are the total skin face sheet thickness and the elastic moduli of the skin's facesheet material (E_{xx}, E_{yy}, and G_{xy}), which is assumed to be transversely isotropic ($E_{zz} = E_{yy}$, $G_{xz} = G_{yz} = G_{xy}$). The core thickness for each group is defined as a design variable in the middle level. The eight ribs divide the wing into an equal number of sections with all the spars in each section having equal thicknesses. Each rib is also assumed to have a uniform thickness.

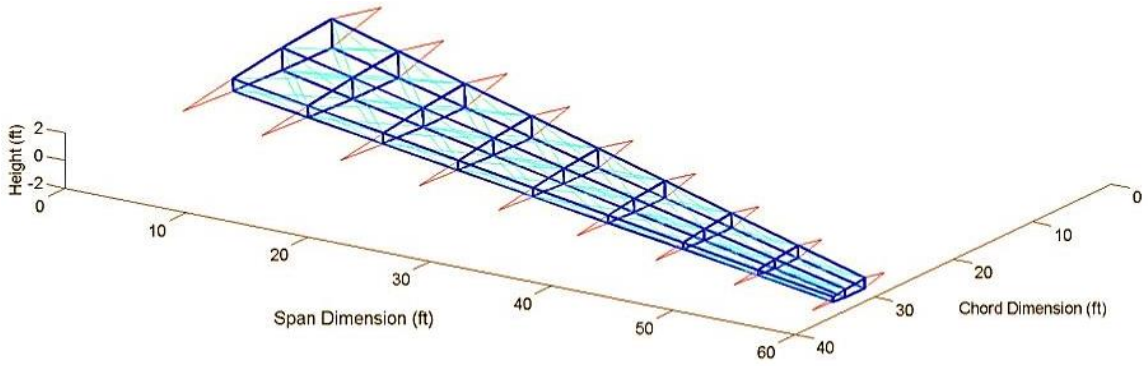

Figure 7.4 The finite element model of the wing

The loading on the wing is meant to represent a 3.75 g pull-up maneuver, the FAA requirement for a transport wing's ultimate load (Federal Aviation Regulations Part 25). The maximum gross takeoff weight of the aircraft is assumed to be 300,000 lb. More information about the specifications of the aircraft and the wing is provided in Table 7.1. The forces applied to the wing are distributed in both the chordwise and spanwise directions to simulate the aerodynamic forces. For this simulation, forces associated with engine thrust and weight as well as structural and fuel weights are not considered. The chordwise distribution of the aerodynamic loads is shown in Figure 7.5. The horizontal force applied to the leading edge node simulates the drag force and is applied to the leading edge only. The spanwise distribution is shown in Figure 7.6. To find the force on any given node, the wing section load (31,887.76 lb) is multiplied by the corresponding spanwise and chordwise coefficients. For example, the nodal force applied to the node at the rear spar on rib 5 is $F_{5,4} = 31{,}887.76 \text{ lb} * 0.7 * 0.5 = 11{,}160.72 \text{ lb}$ where the subscripts 5 and 4 represent the rib number and chord position, respectively.

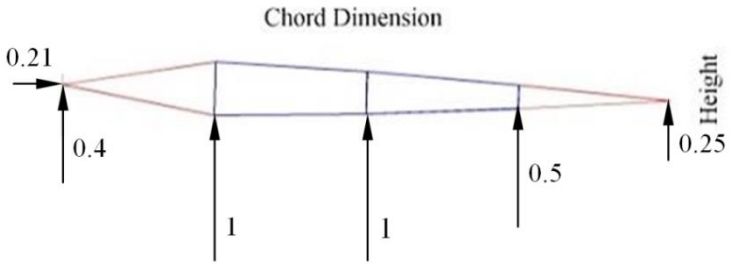

Figure 7.5 Normalized chordwise lift distribution

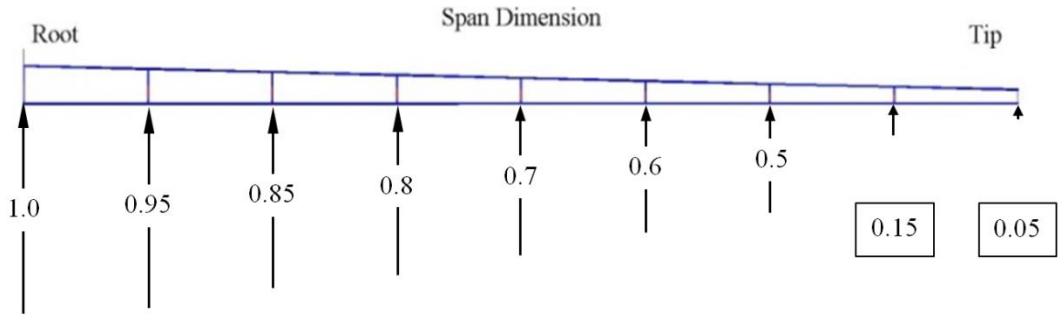

Figure 7.6 Normalized spanwise lift distribution

Table 7.1 Transport Aircraft and Wing Specifications

Property	*Symbol*	*Value*	*Units*
Gross Takeoff Weight	GTOW	300,000	lb
Ultimate Load Factor of Safety		FS_U	3.75
Wing Area	S_w	2,100	ft^2
Wing Span	b_w	120	ft
Root Chord	c_r	25	ft
Rib Spacing	l_{panel}	7.5	ft
Leading Edge Sweep	Λ_{LE}	25.6	degrees
Aspect Ratio	AR	6.86	
Taper Ratio	λ	0.4	
Airfoil Thickness Ratio	t/c	0.15	

The optimization algorithm defines the face sheet properties. To apply them to the NASTRAN CQUAD elements in a meaningful way, a MAT8 material card is used to define a new custom material with the selected moduli. This user defined material is then applied to each skin element using the PCOMP property card. The top face sheet layer thickness is one-half of the total face sheet thickness, t_{fs}; the core thickness is defined by Level 2 and merely inserted in the middle layer of the PCOMP, and the bottom face sheet has the same thickness as the top and uses the same user defined material. The core material is assumed to have moduli of $E_c = 1.3\ ksi$ and $G_c = 1.2\ ksi$ with an assumed

effective density of $\rho_c = 5\ lb/ft^3$ in this level. The moduli are approximately the same as those for Divinycell F40 and the effective density is approximately that of aluminum honeycombs, similar to the one designed at Level 2. These approximations are valid because the core related failure modes are calculated in Level 2 and the core properties are so much smaller than the face sheet properties that their influence on this level is negligible. This approximation also does not affect the weight calculations in a way that would change the optimization, because the assumed effective core density is approximately the same as the actual density and is much less than the material density of either aluminum or carbon fiber composites.

The optimization problem in Element 11 at the top level is expressed as

$$\begin{aligned}
&\min_{t_{fs},ts,tr,E_{xx},E_{yy},G_{xy}} \ \sum_{i=1}^{n_{panel}}[\rho_{cf}\ (Ap_i\ t_{fs_i}) + \rho_c\ (Ap_i\ h_{c_i})] \\
&\qquad +\rho_{Al}\ \sum_{j=1}^{m}(As_j\ ts_j + Ar_j\ tr_j) + \pi_{EPF} \\
&s.t.\ \ g_1 = \delta_{tip} - 16\ ft\ \leq 0 \\
&\qquad g_2 = \theta_{tip} - 3\ deg\ \leq 0 \\
&\qquad g_3 = 50\ ksi - \sigma_{CompMax} \leq 0 \\
&\qquad g_4 = \sigma_{TenMax} - 25\ ksi \leq 0 \\
&0.2\ in \leq t_{fs} \leq 4\ in\ ;\ 0.4\ in \leq ts \leq 5\ in\ ;\ 0.2\ in \leq tr \leq 4\ in\ ; \\
&2{,}057\ ksi \leq E_{xx} \leq 20{,}739\ ksi\ ;\ \ 2{,}057\ ksi \leq E_{yy} \leq 20{,}739\ ksi\ ; \\
&\qquad 822\ ksi\ \leq G_{xy} \leq 5{,}465\ ksi
\end{aligned} \tag{7.1}$$

where n_{panel} is the number of skin panel groups, m is the number of spar and rib groups, $\rho_{cf} = 124.4\ lb/ft^3$ is the density of the carbon fiber composite, ρ_c is the assumed

effective density of the core, and $\rho_{Al} = 168.6\ lb/ft^3$ is the density of 6061 aluminum alloy. The thicknesses of the face sheets, cores, spars, and ribs are denoted by t_{fs}, h_c, ts, and tr, respectively. The core thickness is defined by Level 2 and the other thicknesses are variables. The areas used to calculate the mass of the wing are the area of the panels, Ap, the area of the spar webs, As, and the area of the rib webs, Ar. Constraints are enforced on the maximum tip deflection, δ_{tip}, maximum tip twist angle, θ_{tip}, and the maximum compressive and tensile stresses, $\sigma_{CompMax}$ and σ_{TenMax}, respectively. The material properties of the aluminum used in this problem along with the maximum and minimum properties of the carbon fiber used in the face sheets are shown in Table 7.2 below. The subscripts for the material properties below refer to a laminate based coordinate system where the 1 direction refers to the in plane direction along the short dimension of the panel, 2 refers to the in plane direction along the long dimension of the panel, and 3 refers to the out of plane direction.

Table 7.2 Material Properties for Wing Components

Ply material minimum properties ($V_{CF} = 0.25$, $V_{CNF} = 0.0$)

Property	*Symbol*	*Value*	*Units*	
Longitudinal Elastic Modulus		E_1	16,697.47	ksi
Transverse Elastic Modulus		E_2	675.09	ksi
Shear Modulus	G_{12}	270.77	ksi	
Poisson's Ratio	ν_{12}	0.26		

Ply material maximum properties ($V_{CF} = 0.75$, $V_{CNF} = 0.3$)

Property	*Symbol*	*Value*	*Units*	
Longitudinal Elastic Modulus		E_1	49,524.11	ksi
Transverse Elastic Modulus		E_2	8,305.64	ksi
Shear Modulus	G_{12}	3,194.48	ksi	
Poisson's Ratio	ν_{12}	0.300		

6061 Aluminum Alloy (Spar and Rib Material)

Property	*Symbol*	*Value*	*Units*
Density	ρ_{Al}	168.60	lb/ft^3
Elastic Modulus	E_{Al}	10,000	ksi
Shear Modulus	G_{Al}	3,770	ksi
Poisson's Ratio	ν_{Al}	0.33	
Tensile Strength	$\sigma_{T_{cr}}$	50	ksi
Compressive Strength	$\sigma_{C_{cr}}$	25	ksi

The exponential penalty function formulation in the augmented Lagrangian in Eq. (7.1) is expressed as

$$\pi_{EPF} = \sum_{i=2}^{n_{panel}+1} \{ \frac{\mu_{2\,i}}{a_{2\,i}} \left(e^{a_{2\,i}(t_{2\,i} - r_{2\,i})} - 1 \right) + \frac{\gamma_{2\,i}}{b_{2\,i}} \left(e^{b_{2\,i}(r_{2\,i} - t_{2\,i})} - 1 \right) \} \qquad (7.2)$$

where $\boldsymbol{t}_{2\,i} = [E_{xx}, E_{yy}, G_{xy}, tl]$; $\boldsymbol{r}_{2\,i} = [E^R_{xx}, E^R_{yy}, G^R_{xy}, tl^R]$; $\bar{\boldsymbol{x}}_{11} = [ts, tr]$;

the superscript R denotes responses from Elements 22 and 23, and tl denotes the total laminate thickness $t_l = 2\,t_{fs} + h_c$. It should be noted that the membrane forces are held constant at this level; they are an output of the NASTRAN analysis and are needed in

Elements 22 and 23 for the sandwich failure analyses and determining whether the laminate meets the first ply failure criterion.

Element 22 and 33: Macro-Level Structural Design and Buckling Model

Elements 22 and 23, in the middle level, optimize the mass of the composite sandwich panel treated as simply-supported rectangular sandwich plates under the combined in-plane loading defined by the membrane forces found in Element 11. Elements 22 and 23 optimize to prevent failure of the sandwich through optimization of the core and facesheet properties. The variables for this level are the volume fraction of the carbon fibers, the angles and thicknesses of each facesheet ply, θ_i and t_i, respectively, the foil thickness of the honeycomb core, t_c, the thickness of the core, h_c, and the cell size of the honeycomb, S. These variables are defined graphically in Figure 7.7.

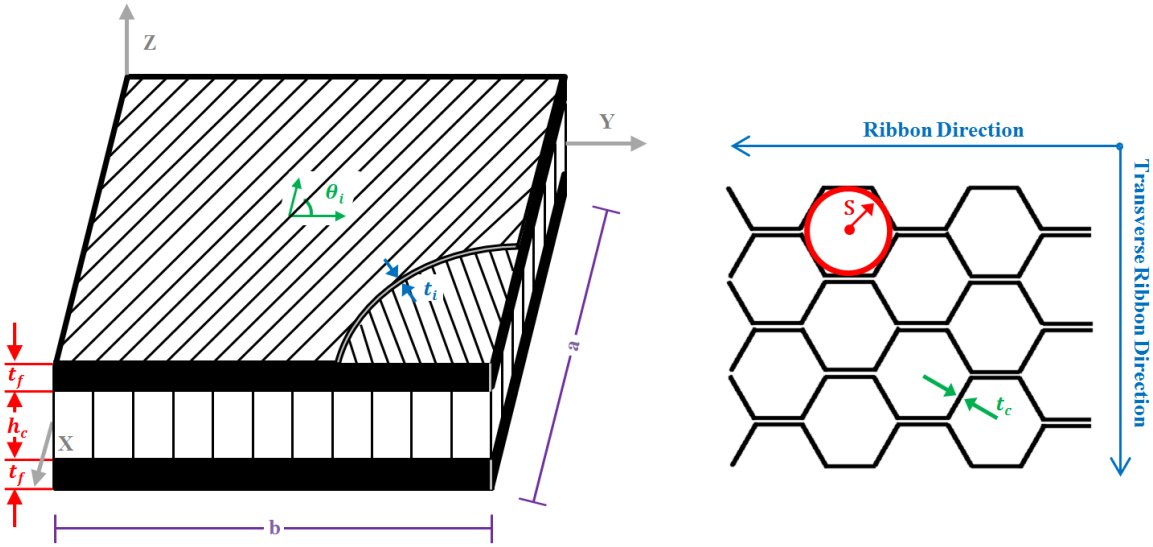

Figure 7.7 Graphical definition of variables in the middle level

Each facesheet laminate is assumed to have 32 plies. The top and bottom face sheets are identical. For simplicity, the 32-layer facesheet is divided into four identical sub-stacks defined by 16 variables (i.e. 8 thicknesses and 8 orientation angles). This pattern is then replicated following the double symmetry to define all 32 plies. While the facesheet is certain to be symmetric, it may not be balanced. This choice of facesheet laminate design was dictated by the limitations of the laminate analysis code used in this research which was developed by Clements (1997). In a more general solution, there is no need to impose a limit on the facesheet ply pattern.

The panels, as defined in Element 11, are from a swept, tapered wing, giving swept or oblique, tapered panels that have only one set of parallel sides (defined by the ribs) and no right angled corners. The laminate analysis code used in this element is for rectangular plates. To find a rectangular plate that closely approximates the actual wing panel, the parallel sides are averaged to give the short dimension, and the long dimension (the distance between the ribs) is maintained at 90 inches. This gives a rectangular plate of the same area and approximately the same dimensions as the original. An example of this transformation is shown in Figure 7.7 where the original panel 1 is shown in red outline and the rectangular approximation is shown in blue.

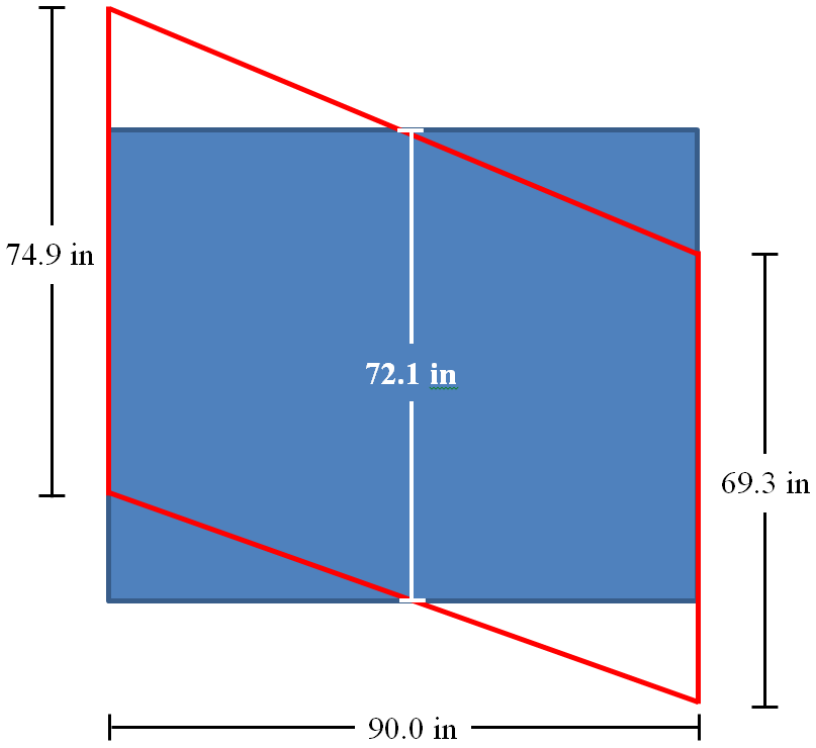

Figure 7.8 Comparison of the original panel 1 and its rectangular approximation Original panel 1 in red. Rectangular approximation for buckling analysis in blue.

Oblique, tapered panels have different, but predictable, global buckling load and mode shape. Whittrick (1953) and Timoshenko and Gere (1961) provide the buckling analysis for simply supported oblique panels with sweep angles of 30° and 45°. The front edge sweep angle of the wing panels is 19.5° and the rear edge sweep is 16.3° for an average of 17.9°. There is no information for angles less than 30°; however, the buckling strength of an oblique panel with a sweep angle of 30° is shown to be 25 % less than a rectangular plate of the same area. Pope (1962) showed the effect of taper on a panel's global buckling load. He showed that taper increases the stress required for global buckling when one side is reduced and the other maintains its original dimension. Using the data in that paper, it is estimated that the critical global buckling stress is increased by

a minimum of 10 % for panels of the geometry tested here, offsetting the reduction from the sweep. Given the geometry of the panels under consideration, the two effects will nearly or completely offset each other, so it is reasonable to approximate each wing panel as a rectangular plate in the way described above. The failure modes considered for the panel are first ply failure, plate buckling, shear crimping, facesheet dimpling, and facesheet wrinkling.

First ply failure approach examines each ply in the laminate to determine failure using the selected failure criterion (e.g. max strain, Tsai-Hill, Tsai-Wu) (Agarwal et. al. 2006, Vinson and Sierakowski 1986). In this case, the max strain failure criterion is used, which requires determination of the local strains in the principal material directions of each unidirectional ply and their comparison with the corresponding maximum strain allowables. The ultimate stresses are noted with the other material properties in Table 7.3. The material exhibits differing behavior in the longitudinal and transverse directions as well as in tension and compression; therefore, there are five different ultimate strain values calculated as

$$\varepsilon_{1t_u} = \frac{\sigma_{1t_u}}{E_1} \; ; \quad \varepsilon_{2t_u} = \frac{\sigma_{2t_u}}{E_2} \; ; \quad \varepsilon_{1c_u} = \frac{\sigma_{1c_u}}{E_1} \; ; \quad \varepsilon_{2c_u} = \frac{\sigma_{2c_u}}{E_2} \; ; \quad \gamma_{12_u} = \frac{\tau_{12_u}}{G_{12}} \qquad (7.3)$$

where subscripts 1 or 2 refer to the ply or in-plane principle and transverse direction, respectively, subscripts t or c refer to tensile or compressive, respectively, ε refers to normal strains, and γ refers to shear strain. Since there are two ultimate normal strains for each direction, the critical allowable is the one that matches the loading indicated by the sign of the calculated ply strain where a negative sign indicates compression.

Table 7.3 Material Properties for Face Sheet Components

Carbon Fibers

Property	*Symbol*	*Value*	*Units*
Elastic Modulus	E_f	65,266.98	ksi
Shear Modulus	G_f	25,102.69	ksi
Poisson's Ratio	ν_f	0.300	

Neat Matrix

Property	*Symbol*	*Value*	*Units*
Elastic Modulus	E_m	507.63	ksi
Shear Modulus	G_m	203.62	ksi
Poisson's Ratio	ν_m	0.300	

Matrix with $V_{CNF} = 0.3$

Property	*Symbol*	*Value*	*Units*
Elastic Modulus	E_{NEM}	2,295.50	ksi
Shear Modulus	G_{NEM}	882.88	ksi
Poisson's Ratio	ν_{NEM}	0.247	

Constant Ply Properties

Property	*Symbol*	*Value*	*Units*
Density	ρ_c	124.4	lb/ft^3
Longitudinal Tensile Strength	σ_{1t_u}	410.0	ksi
Transverse Tensile Strength	σ_{2t_u}	7.1	ksi
Compressive Strength	σ_{1c_u}	-270.0	ksi
Transverse Compressive Strength	σ_{2c_u}	-36.0	ksi
Shear Strength	τ_{12_u}	12.0	ksi

2024 Aluminum Alloy (Core material)

Property	*Symbol*	*Value*	*Units*
Elastic Modulus	E_c	10,000	ksi
Shear Modulus	G_c	3,846.15	ksi
Poisson's Ratio	ν_c	0.300	

Global buckling is the buckling of the entire panel as a single unit. This buckling mode is defined primarily by the equivalent Young's modulus of the facesheet and the moment of inertia of the panel in both the x and y directions. The moment of inertia, in turn, is controlled by the thickness and moduli of the individual plies and the thickness of the core. The principle of minimum total potential energy is used to find the buckling

loads ($N_{x_{cr}}, N_{y_{cr}}, N_{xy_{cr}}$) as described by Clements (1997) and Rais-Rohani and Marcellier (1999). The corresponding buckling stresses are found as

$$\sigma_{x_{cr}}^{gb} = \frac{N_{x_{gb}}}{2\,t_{fs}}\ ; \quad \sigma_{y_{cr}}^{gb} = \frac{N_{y_{gb}}}{2\,t_{fs}}\ ; \quad \tau_{xy_{cr}}^{gb} = \frac{N_{xy_{gb}}}{2\,t_{fs}} \tag{7.4}$$

Shear crimping is caused by insufficient core shear stiffness resulting in localized core buckling and a crimp in the sandwich plate. The core permanently fails at the crimp meaning this is not an elastic buckling mode. The critical shear crimping stresses are found as (Bruhn 1973, Vinson and Sierakowski 1986)

$$\sigma_{x_{cr}}^{sc} = \frac{2}{3}\frac{t_c\,h_c\,G_c}{S\,t_{fs}};\ \sigma_{y_{cr}}^{sc} = \frac{4}{15}\frac{t_c\,h_c\,G_c}{S\,t_{fs}}\ ;\ \tau_{xy_{cr}}^{sc} = \sqrt{\frac{8}{45}}\frac{t_c\,h_c\,G_c}{S\,t_{fs}}\ ; \tag{7.5}$$

where G_c is the shear modulus of the core material (2024 Aluminum Alloy). The difference between the x critical stress and the y critical stress is that the panel is assumed to be oriented with the ribbon direction of the foil oriented in the x direction. Here, Vinson and Sierakowski's (1986) equations are used to calculate the effective core shear modulus resulting in a slightly lower critical x stress and a transverse ribbon direction critical stress that is 40 % of the ribbon direction instead of Bruhn's (1973) suggested 70 %. Vinson and Sierakowski's (1986) criteria for distinguishing global buckling from shear crimping are also used in this analysis as described by Clements (1997).

Facesheet dimpling, also called intracell buckling, is a special type of local buckling in which the buckling "panel" is defined by the edges of the honeycomb cell. This mode usually occurs when the facesheet is thin compared to the honeycomb cell size. It derives its name from the small round buckling regions resembling the dimpled

surface of a golf ball. While this mode may not lead to catastrophic failure (Bruhn 1973 & Vinson and Sierakowski 1986), it is considered in that way for this study, because it can also disturb the aerodynamic performance of the wing skin. The critical value is calculated as (Vinson and Sierakowski 1986)

$$\sigma_{cr}^{ib} = \frac{2\sqrt{\bar{E}_{xx}\,\bar{E}_{yy}}}{1-\bar{\nu}_{xy}\,\bar{\nu}_{yx}} \left(\frac{t_{fs}}{S}\right)^2 \tag{7.6}$$

where $\bar{E}_{xx}$ and $\bar{E}_{yy}$ are the approximate values of Young's modulus in the x and y direction calculated using the in-plane stiffness matrix by the equations $\bar{E}_{xx} = \frac{A_{11}}{t_{fs}}\left[1 - \frac{{A_{12}}^2}{A_{11}\,A_{22}}\right]$ and $\bar{E}_{yy} = \frac{A_{22}}{t_{fs}}\left[1 - \frac{{A_{12}}^2}{A_{11}\,A_{22}}\right]$. The A matrix used in these equations comes from classical lamination theory (Agarwal et al. 2006).

Facesheet wrinkling is a local buckling of the face sheet in which part of the face sheet either rips away from the core or crushes the core. This mode usually occurs when the face sheets are insufficiently thin compared to the core thickness. The face sheets then buckle while the core does not causing the face sheets to separate from the core if the bond with the core is critical or crush the core if core compression is critical. The critical stress is defined as (Vinson and Sierakowski 1986)

$$\sigma_{cr}^{w} = \tau_{cr}^{w} = \sqrt{\frac{16\,t_{fs}\,t_c\,E_c'\sqrt{\bar{E}_{xx}\,\bar{E}_{yy}}}{9\,h_c\,S\left(1-\bar{\nu}_{xy}\,\bar{\nu}_{yx}\right)}} \tag{7.7}$$

where E_c' is the core stiffness in the z direction calculated as $E_c' = 2.13\left(\frac{3\,t_c}{S}\right)^{1.416} E_c$ (Bruhn 1973).

Equations 7.3, 7.4, 7.5, 7.6, and 7.7 are implemented inside a FORTRAN code (Clements 1997) which considers each failure mode as a constraint and evaluates the mass of the panel. Each failure criterion has a set range of $[-\infty, 1]$ where values greater than zero indicate safe designs. These failure mode evaluations are denoted here as g_{fpf}, g_{gb}, g_{sc}, g_{ib}, and g_w for the constraints on first ply failure, global buckling, shear crimping, intracell buckling, and facesheet wrinkling, respectively.

Only the critical panel is tested for each panel group with the critical panel being the most forward and closest to the root as shown in Figure 7.3. If the upper and lower skins are considered in the same group, the upper skin is considered the critical panel, since it is under compressive load and the composite is weaker in compression than in tension. The optimization problem in Elements 22 and 23 shown in Figure 7.3 are expressed as

$$\min_{V_{CF},E_{NEM},\upsilon_{NEM},\theta_i,t_i,h_c,t_c,S} W_{panel} + w_1\left(\frac{E_{NEM}^{T}-E_{NEM}^{min}}{E_{NEM}^{max}-E_{NEM}^{min}}\right) + w_2 V_{CF} + \pi_{EPF}$$

$$s.t.\ \ g_{fpf} \geq 0$$

$$g_{gb} \geq 0$$

$$g_{sc} \geq 0$$

$$g_{ib} \geq 0 \qquad (7.8)$$

$$g_w \geq 0$$

$$0.25 \leq V_{CF} \leq 0.75;\ \ 500 \leq E_{NEM} \leq 2{,}300\ ksi;\ \ 0.247 \leq \upsilon_{NEM} \leq 0.3;$$

$$0.005 \leq t_i \leq 0.6\ in;\ \ -90^o \leq \theta_i \leq 90^o\ ;\ \ 0.1 \leq h_c \leq 5.0\ in\ ;$$

$$0.0007 \leq t_c \leq 0.1\ in\ ;\ \ 0.0625 \leq S \leq 2.0\ in$$

where properties with the subscript NEM refer to those associated with the nano-enhanced matrix whereas w_1 and w_2 are weights representing the manufacturing costs associated with increasing the volume fraction of the carbon nanofibers in the matrix (which causes an increase in the Young's modulus at this level) or the volume fraction of the continuous carbon fibers reinforcing the nano-enhanced matrix.

The exponential penalty function for Elements 22 and 23 is expressed as

$$\begin{aligned}\pi_{EPF} &= \frac{\mu_{2\,j}}{a_{2\,j}}\left(e^{a_{2\,j}\,(\boldsymbol{t}_{2\,j}-\boldsymbol{r}_{2\,j})}-1\right)+\frac{\gamma_{2\,j}}{b_{2\,j}}\left(e^{b_{2\,j}\,(\boldsymbol{r}_{2\,j}-\boldsymbol{t}_{2\,j})}-1\right)\\ &\quad+\frac{\mu_{3\,k}}{a_{3\,k}}\left(e^{a_{3\,k}\,(\boldsymbol{t}_{3\,k}-\boldsymbol{r}_{3\,k})}-1\right)+\frac{\gamma_{3\,k}}{b_{3\,k}}\left(e^{b_{3\,k}\,(\boldsymbol{r}_{3\,k}-\boldsymbol{t}_{3\,k})}-1\right)\\ \boldsymbol{t}_{2\,j} &= \left[E_{xx}^{T},E_{yy}^{T},G_{xy}^{T},tl^{T}\right];\quad \boldsymbol{r}_{2\,j}=[E_{xx},E_{yy},G_{xy},tl];\quad \boldsymbol{t}_{3\,k}=[E_{NEM},\nu_{NEM}];\\ \boldsymbol{r}_{3\,k} &= [E_{NEM}^{R},\nu_{NEM}^{R}];\quad \bar{\boldsymbol{x}}_{2\,j}=[V_{CF},t_i,\theta_i,h_c,t_c,S]\end{aligned} \tag{7.9}$$

where $j = n_{panel} + 1$ and $k = 2\,n_{panel} + 1$, with n_{panel} as the number of panel groups, the superscripts T and R designate target and response values delivered from Element 11 and Element $3k$, respectively, and the response moduli are the outputs of the laminate analysis code.

Element 34 and 35: Micro-Level Material Model Analysis and Design

In Element 34 and 35 at the bottom level in Figure 7.3, the matrix material is enhanced through the addition of carbon nano-fibers (CNFs). The purpose is to optimize the volume fraction of CNFs, V_{CNF}, to meet the target values for the Young's modulus and Poisson's ratio set in Elements 22 and 23. Though the optimization itself has a simple formulation, the model used to determine the Young's modulus and Poisson's ratio is quite complicated.

The model assumes randomly oriented wavy CNFs that are surrounded by a three-dimensional interphase region with properties modeled using functionally graded representation. The general approach is based on Mori-Tanaka homogenization and Eshelby's ellipsoidal inclusion model to find the effective modulus of the enhanced matrix (E_{NEM}). Rouhi et al. (2010) examined the effects of volume fraction (V_{CNF}) and aspect ratio on the enhanced modulus. One important point of examination in their work was the use of a non-homogenous interphase region, the portion of the matrix in very close proximity to the fiber that behaves differently than either the fiber or the matrix. They used the multi-inclusion approach developed by Nemat-Nasser and Hori (1993) to create "layers" of homogenous interphase region around the nano-fiber that give the effect of a non-homogenous interphase region. A property, P, for "layer" α is given as

$$P = P_{in} + (P_{out} - P_{in})\left(\frac{\alpha-1}{N}\right)^n \tag{7.10}$$

where P_{in} is the property's value next to the nano-fiber, P_{out} is the value of the property for the neat matrix, N is the number of "layers" used in the simulation, and n is the interphase variation parameter. α varies from 1 to $N+1$ where $\alpha = 1$ is the layer closest to the nano fiber and $\alpha = N$+1 is outside the interphase. For this simulation P_{in} was chosen as the value of the property for the nano-fiber. A linear variation of the parameter is represented by $n = 1$. For more information on this model see Rouhi et al. (2010), Rouhi (2011), Rouhi and Rais-Rohani (2013), or DorMohammadi (2013). The values used in this analysis are shown in Table 7.4.

Table 7.4 Material Properties for Enhanced Matrix Components

Neat Vinyl Ester Matrix

Property	*Symbol*	*Value*	*Units*
Elastic Modulus	E_m	507.63	ksi
Shear Modulus	G_m	203.62	ksi
Poisson's Ratio	ν_m	0.300	

Carbon Nanofibers

Property	*Symbol*	*Value*	*Units*
Elastic Modulus	E_{CNF}	65,266.98	ksi
Poisson's Ratio	ν_{CNF}	0.300	
Radius	r_{CNF}	0.5	μm
Length	L_{CNF}	259	μm
Waviness Length	λ_{CNF}	150	μm
Waviness Amplitude	A_{CNF}	50	μm

Interphase Region

Property	*Symbol*	*Value*	*Units*
Thickness Ratio	t_{IP}/r_{CNF}	0.5	
Variation Parameter	n	1	(Linear variation)
Number of Homogenous Regions	N	10	
Modulus for $\alpha = 1$	E_{in}	65,266.98	ksi
Modulus for $\alpha = N$	E_{out}	507.63	ksi

The volume fraction of CNFs is the only variable at this level, and the only goal of the optimization is compliance with the target values. The only constraints are the side constraints on the CNF volume fraction. Thus, the objective function is merely the exponential penalty function and the optimization problem in Element 34 and 35 is formulated as

$$\min_{V_{CNF}} \frac{\mu_{3\,k}}{a_{3\,k}}\left(e^{a_{3\,k}\,(t_{3\,k}-r_{3\,k})}-1\right)+\frac{\gamma_{3\,k}}{b_{3\,k}}\left(e^{b_{3\,k}\,(r_{3\,k}-t_{3\,k})}-1\right)$$

$$s.t.\quad 0 \le V_{CNF} \le 0.3 \tag{7.11}$$

$$\boldsymbol{t}_{3\,k}=[E_{NEM}^{T},\nu_{NEM}^{T}];\quad \boldsymbol{r}_{3\,k}=[E_{NEM},\nu_{NEM}];\quad \bar{x}_{3\,k}=V_{CNF}$$

where the responses are the output of the NEM program for the given V_{CNF}. There is no weighting in the objective function at this level. The weighting function in Element 22 and 23 with the target-response process makes it unnecessary. Current processing methods restrict the maximum volume fraction of nano fibers that can be added to a matrix while still increasing mechanical properties to less than 3 %. For this study, it is assumed that these manufacturing limitations do not exist.

Optimization Framework and Results

The decomposition of the optimization problem is shown in Figure 7.8.

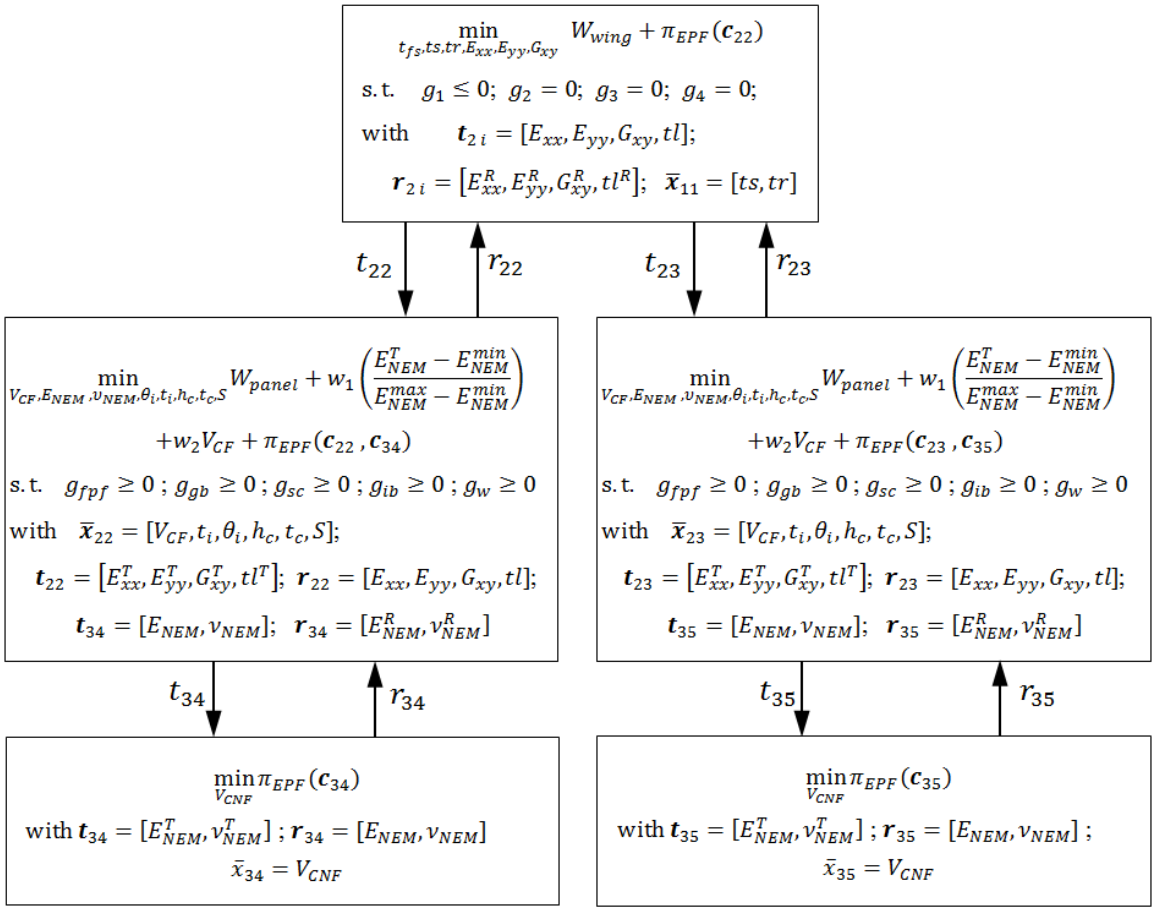

Figure 7.9 Hierarchical decomposition of the two section transport wing problem

The decomposed multilevel wing design optimization problem was organized and solved using VisualDOC (2012). This software provides the necessary tool for testing different optimization frameworks and allows for easy integration of multiple analysis programs and optimization methods within a specified framework. The solution process selected begins at the bottom level working upward to Element 11 at the top. Panel 1 is solved first starting with the NEM problem, Element 34, then moving to the sandwich panel, Element 22, followed by Panel 2 in the same order, and finally the wing level problem, Element 11. The workflow diagram is shown in Figure 7.9 using a screen capture from the main page of the VisualDOC software.

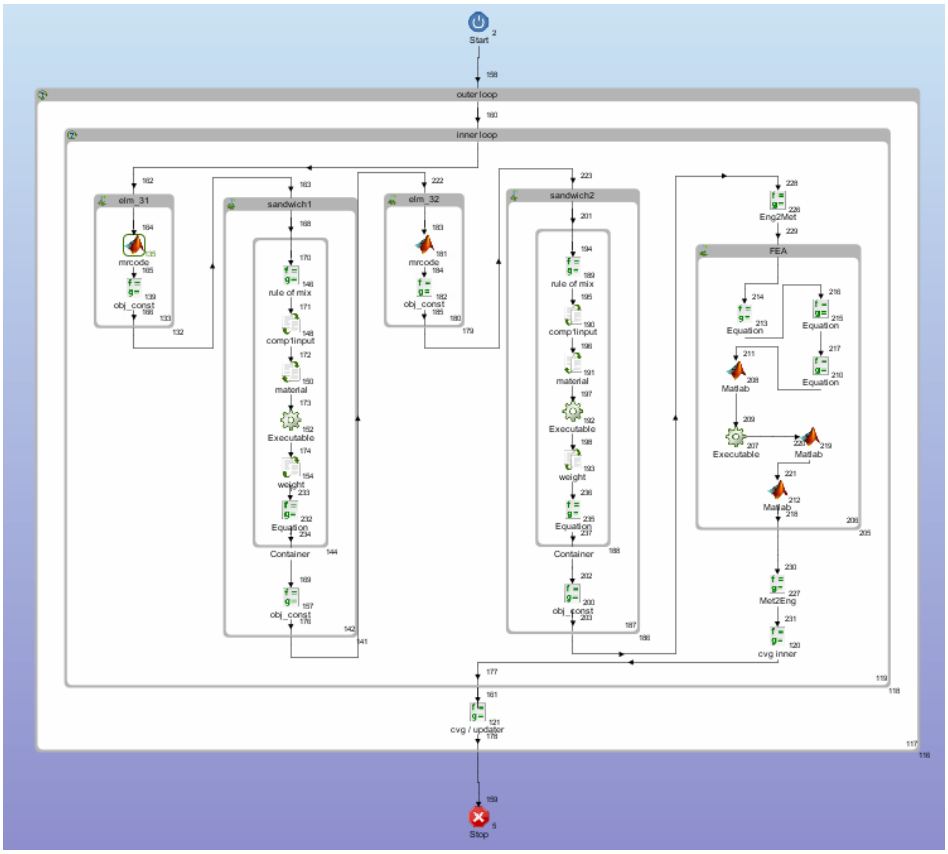

Figure 7.10 The VisualDOC workflow for the Transport Aircraft Wing Optimization

Since the optimization algorithm is performing a non-physics based search trying to optimize the moduli of the panel, the panels at this level can take on unrealistic sets of moduli. The moduli are brought back to realistic values through the optimization by the targets and responses set at different levels by physics based models. By solving the panels before the wing, a realistic response is established for the wing level target to match. The relaxed formulation of the consistency constraint allows the wing level problem to set targets that benefit the wing level, but are still close to a realistic value.

The wing-level problem in Element 11 uses the gradient-based Modified Method of Feasible Directions (MMFD) optimization algorithm. The forward difference method is used to calculate the gradients. This element uses NASTRAN to analyze the finite element model. Also, MATLAB scripts, modified from those used by Parrish (2014), were used to write the input file for the NASTRAN analysis and read the output files to find the rib and spar stresses, the wing deflections, and the panels' membrane forces.

The panel level problems in Elements 22 and 23 use the gradient-based Sequential Linear Programming (SLP) optimization algorithm. Even though this algorithm is not as efficient as MMFD, it is more robust than MMFD which is needed because the constraints at this level have unperceivable or no gradient over parts of the design space. This element referenced the laminate analysis Fortran code written by Clements (1997). The input and output files for this analysis are much simpler, and therefore use a VisualDOC to modify a template of the input file and find the relevant data in the output file.

The nano-enhanced matrix level problem in Elements 34 and 35 also uses MMFD with the analysis routine written in a MATLAB script by Rouhi (2011).

The double loop approach was used on this problem due to its robustness. While a single loop formulation might be faster, its greater sensitivity to initial weights and multipliers is undesirable as even the double loop was quite sensitive. The tolerance for this problem was set at $\tau = 0.01$ for both the inner and outer loops. The EPF formulation used initial multipliers of $\boldsymbol{\mu}_{ij} = \boldsymbol{\gamma}_{ij} = 1$ for all multipliers.

An initial weight of $\boldsymbol{a}_{ij} = \boldsymbol{b}_{ij} = 1$ was used for the Element 22/Element 34 and Element 23/Element 35 interactions with that being increased to 1.2 for the Element 11/Element 22 and the Element 11/Element 23 interactions due to more specialized, very different solutions to each level's problem. An updating factor of $\beta = 1.2$ was used. This unique set of initial weights and updating factor values was derived from trial and error. It was discovered during the implementation process that the critical constraints for the problem were allowable wing twist at the top level and global buckling and first ply failure in the sandwich plate level. The solution to the top level problem was panels with high shear stiffness. The solution to the sandwich plate level problem was panels with plies oriented mainly in the direction of maximum loading (i.e., panels with a high longitudinal stiffness in the primary loading direction). It was found that if the initial weights and updating factors were too low, the inner and outer loops would converge to a solution without proper target-response coordination. Conversely, if the initial weights or updating factors were too high, the problem would initially converge. The updater would then update the multipliers to force convergence. Because the updating of the multipliers is heavily dependent on the weights, they would be updated to values that caused them to push too hard. The targets would then overshoot the responses and vice versa. This led to a divergent oscillation of the targets and responses. Thus, the initial weights and updating

factors needed to be carefully selected for this problem. This phenomenon was not observed in any other problem tested.

The initial values for the wing are reported in Table 7.5 and the initial values for the panels are reported in Table 7.6. Though both panels are vastly different, they used the same initial values. The initial design point does not meet all stated constraints for this problem, so it is not an accurate comparison to compare it to the optimized wing. Without uncertainty, meeting the constraints is not a requirement of the initial point. The variables for the optimized wing are also shown in Table 7.5 and two optimum panels are shown in Table 7.6. Since the top level problem solved here is merely a sub-problem of the one solved by Garcelon et. al (1999), Venter and Sobieszczanski-Sobieski (2006), and Parrish (2014), there is no published data on the objective function to use for comparison.

Table 7.5 Design variable values for Element 11

Design Variable	Lower Bound	Initial Value	Optimum	Upper Bound	Units
Panel Group 1					
E_{xx}	675.09	14,894.85	3,983.21	49,524.11	ksi
E_{yy}	675.09	14,894.85	2,212.97	49,524.11	ksi
G_{xy}	270.77	5,899.12	7,804.64	18,920.02	ksi
t_{fs}	0.189	0.4	0.189	4.0	in
Panel Group 2					
E_{xx}	675.09	14,894.85	1,890.38	49,524.11	ksi
E_{yy}	675.09	14,894.85	7,164.03	49,524.11	ksi
G_{xy}	270.77	5,899.12	4,321.02	18,920.02	ksi
t_{fs}	0.157	0.4	0.157	4.0	in
Spar/Rib Group 1					
ts	0.394	0.43	1.043	5.0	in
tr	0.197	0.2	0.197	4.0	in
Spar/Rib Group 2					
ts	0.394	0.43	0.836	5.0	in
tr	0.118	0.122	0.127	4.0	in
Wing Weight	**3,505.89**	**5,883.14**	**4,755.49**	**-**	**lb**

Table 7.6 Design variable values of the optimized panels

Design Variable	Lower Bound	Initial Value	Panel 1 Opt	Panel 2 Opt	Upper Bound	Units
V_{CNF}	0.001	0.1	0.0610	0.0013	0.3	-
V_{CF}	0.25	0.3	0.4844	0.6488	0.75	-
E_{NEM}	507.63	725	891.3	512.4	2,295.5	ksi
ν_{NEM}	0.2465	0.27	0.2721	0.2991	0.3	-
t_1	0.005 *	0.12	0.006	0.005	0.6	Inches
t_2	0.005 *	0.12	0.006	0.005	0.6	Inches
t_3	0.005 *	0.12	0.006	0.005	0.6	Inches
t_4	0.005 *	0.12	0.006	0.005	0.6	Inches
t_5	0.005 *	0.12	0.006	0.005	0.6	Inches
t_6	0.005 *	0.12	0.006	0.005	0.6	Inches
t_7	0.005 *	0.12	0.006	0.005	0.6	Inches
t_8	0.005 *	0.12	0.006	0.005	0.6	Inches
θ_1	-90	0	-38.6	-15.3	90	Degrees
θ_2	-90	-45	-48.6	-15.6	90	Degrees
θ_3	-90	45	40.7	-8.4	90	Degrees
θ_4	-90	90	40.7	80.9	90	Degrees
θ_5	-90	90	42.1	33.0	90	Degrees
θ_6	-90	45	35.7	-8.8	90	Degrees
θ_7	-90	-45	-48.6	-38.0	90	Degrees
θ_8	-90	0	-38.2	-38.0	90	Degrees
h_c	0.1	0.5	0.1014	0.1	5.0	Inches
S	0.0625	0.5	0.0625	0.0625	5.0	Inches
t_c	0.0007	0.003	0.0007	0.0007	0.01	Inches
Weight	**-**	**-**	**91.23**	**52.51**	**-**	**Pounds**

A lower bound of 0.006 inches was used for panel group 1 (the inboard group)

These results show the difference in the optimal approach to the two panels. Due to their location in the wing, the panels have two very different loadings which lead to very different optimal layups. It is also noted that the optimum ply thicknesses are all at their minimum values and that several plies share a common orientation. This indicates that a reduction in the number of plies would be beneficial. Unfortunately, this avenue cannot be properly explored using the sandwich plate analysis software currently available for this problem. It is also interesting to note that the outboard portion of the

wing had a higher optimal volume fraction of continuous carbon fibers. Even though the ply thicknesses were allowed to be thinner in that portion of the wing, the loading is also lower. Another interesting result is the low volume fraction of the carbon nano-fibers compared to the allowable maximum. The enhancements provided by increased V_{CNF} are outweighed by the artificial cost factor added in Level 2 of this problem.

In total, this problem took approximately 189,000 seconds (= 52.55 hours = 2.19 days) to execute. In comparison, the multilevel sandwich plate reported by DorMohammadi (2013) took 6 hours. For the wing problem, 3 outer loops, 10 inner loops, 392 function calls to the NEM program, 25,403 calls to the sandwich plate analysis, and 2,183 FE analyses were completed. The all-at-once formulation of this problem is expected to take weeks of computational time. The large gain in computational efficiency comes from the concentration of the majority of the variables in the element with the cheap sandwich plate analysis and the isolation of the costly NEM analysis in Elements 34 and 35 where there is only one design variable.

Table 7.7 shows the 12 target-response pairs for this formulation, and their normalized consistency constraint values. This table shows that a coordinated result was achieved by the optimization and that this solution is valid. If these were not converged, the solution would not have any physical relevance. The normalized consistency constraint shows that all target-response pairs were close to the set tolerance with most being below tolerance. Though this was not imposed as a requirement for convergence, it shows the quality of the result.

Table 7.7 Target and response values for the transport aircraft wing problem

Value	Target	Response	Units	Consistency Constraint
Element 11 & 22 (Inboard panel group)				
E_{xx}	3,983.21	3,675.10	ksi	0.0102
E_{yy}	2,212.97	2,542.50	ksi	-0.0110
G_{xy}	7,804.64	7,694.80	ksi	0.0037
tl	0.2903	0.293	in	-0.0006
Element 11 & 23 (Outboard panel group)				
E_{xx}	18,903.81	18,848.00	ksi	0.0019
E_{yy}	7,164.03	7,404.30	ksi	-0.0080
G_{xy}	4,321.02	3,965.3	ksi	0.0119
tl	0.2575	0.2600	in	-0.0005
Element 22 & 34 (Inboard spar/rib group)				
E_{NEM}	868.65	891.25	ksi	-0.0126
ν_{NEM}	0.2719	0.272	-	-0.0042
Element 23 & 35 (Outboard spar/rib group)				
E_{NEM}	515.24	512.37	ksi	0.0016
ν_{NEM}	0.2991	0.2991	-	0.0004

CHAPTER VIII

CONCLUSIONS AND FUTURE WORK

A method was developed for multilevel design optimization of hierarchical systems with epistemic uncertainty using evidence theory. The Evidence-Based Multilevel Design Optimization (EBMLDO) method was then used to solve several non-deterministic optimization problems using analytical functions affected by interval-based uncertainty. The results showed that the solution time increased significantly due to the addition of uncertainty, and the optimum objective function values became more conservative since uncertainty forces the optimum design point to be farther away from the constraint boundaries in comparison to the deterministic solution.

The EBMLDO method was used to explore the effect of belief structure associated with the uncertain variables on the optimized solution. A number of different belief structures of various forms were tested to identify the effect of the belief structure on the optimized solutions. Once the effect of various changes to the belief structure was observed, it was theorized that the most significant aspect of a belief structure was its cumulative plausibility function failure. This theory was tested by creating different belief structures that produced the same cumulative plausibility function as the original belief structure. Then, two theories on the reduction of computational cost were tested by creating a third belief structure to determine if the same results as the original belief

structure could be obtained. This structure did and with a significant reduction in computational costs traced to both theories being tested.

The Transport Aircraft Wing (TAW) example was solved using decomposed multilevel optimization. This problem is more complex than those involving analytical functions and it's solution displayed the power of the multilevel framework to solve complex problems in an efficient manner. This problem includes several "black box" analyses that show the system is able to handle these complex types of analyses.

Future work on multilevel optimization will be to team with industry to solve problems for actual products. Researchers can create increasingly more complex problems to solve with ATC, but until it is implemented on an actual product, the method will not be viewed as mature. This work shows that necessary groundwork is in place to make this next step.

Multilevel optimization under epistemic uncertainty is still an evolving field. The methods set forth in this thesis need to undergo further testing and refinement. Additional refinement is needed to decrease the computational costs. A large step in that effort would be a method that would allow the use of a gradient based optimization algorithm. Another would be a method to calculate the plausibility of failure more efficiently. Eventually, EBMLDO needs to become more computationally efficient to solve problems such as the TAW problem under epistemic uncertainty.

Other questions remain in design optimization under uncertainty. There is a large debate as to whether RBDO has to make too many assumptions to produce a viable answer. Some propose using a more complex version of RBDO, while others think that different uncertainty quantification methods should be employed. I believe the answer

will only come out through having several experts use several of these methods to solve the same simple, real world problems. Data needs to be collected on these problems as it would for an actual problem, with increasing size of the data sets used to quantify the uncertainty. This will allow the assumptions about epistemic uncertainty in the techniques that handle that uncertainty to be tested. Then, these real world problems must be tested a large number of times to gain statistical data on the solution and determine which method returned the most accurate solution. This method has been used before in fatigue testing, but it is quite a costly undertaking. However, I believe it is the only way to answer this question.

REFERENCES

Agarwal, H., Renaud, J.E., Preston, E.L., and Padmanabhan, D., "Uncertainty Quantification Using Evidence Theory in Multidisciplinary Design Optimization," *Reliability Engineering and System Safety*, Vol. 85, pp. 281-294, 2004.

Agarwal, B.D., Broutman, L.J., and Chandrashekhara, K., *Analysis and Performance of Fiber Composites*, 3rd ed., Wiley Press, Hoboken, NJ, 2006.

Allison, J., Kokkolaras, M., Zawislak, M., and Papalambros, P.Y., "On the Use of Analytical Target Cascading and Collaborative Optimization for Complex System Design," Proceedings of the 6th World Congress on Structural and Multidisciplinary Optimization, Rio de Janeiro, Brazil, May 30 - June 3, 2005.

Allison, J., Walsh, D., Kokkolaras, M., Papalambros, P.Y., and Cartmell, M., "Analytical Target Cascading in Aircraft Design," Proceedings of the 44th AIAA Aerospace Sciences Meeting and Exhibit, Reno, NV, Jan. 9-12, 2006.

Bae, H.-R., Grandhi, R.V., and Canfield, R.A., "Epistemic Uncertainty Quantification Techniques Including Evidence Theory for Large-Scale Structures," *Computers and Structures*, Vol. 82, No. 13, pp. 1101-1112, 2004.

Bae, H.-R., Grandhi, R.V., and Canfield, R.A., "Sensitivity Analysis of Structural Response Uncertainty Propagation Using Evidence Theory," *Structural and Multidisciplinary Optimization*, Vol. 31, No. 4, pp. 270-279, 2006.

Ben-Haim, Y., *Information-gap Decision Theory: Decisions Under Severe Uncertainty*, Academic Press, London, 2001.

Berger, J.O., *Decision Theory and Bayesian Analysis*, Springer-Verlag, New York, 1985.

Bruhn, E.F., *Analysis and Design of Flight Vehicle Structures*, 2nd ed. Jacobs, Carmel, IN, Chap. C12, 1973.

Choi, K.K., Du, L., and Youn, B.D., "A New Fuzzy Analysis Method for Possibility-Based Design Optimization," 10th AIAA/ISSMO Multidisciplinary Analysis and Optimization Conference, Albany, NY, August 30-September 1, 2004.

Choquet, G., "Theory of Capacities," *Annales de L'Institut Fourier*, Vol. 5, pp. 131 – 295, 1953.

Clements, T.M., "Global-Local Analysis and Design Optimization of a Composite Tilt-Rotor Wing Box Structure," Master's Thesis, Dept. of Aerospace Engineering, Mississippi State Univ., Starkville, MS, 1997.

Demster, A.P., "A Generalization of Bayesian Inference," *Journal of the Royal Statistical Society*, Series B, Vol. 30, pp. 205-247, 1968.

DorMohammadi, S., and Rais-Rohani, M., "Reliability-Based Design Optimization Within Analytical Target Cascading Framework," Proceedings of the 53rd AIAA/ASME/ASCE/AHS/ASC Structures, Structural Dynamics, and Materials Conference, Honolulu, HI, Apr. 23-26, 2012.

DorMohammadi, S. and Rais-Rohani, M., "Exponential Penalty Function Formulation for Multilevel Optimization Using the Analytical Target Cascading Framework," *Structural and Multidisciplinary Optimization*, Vol. 47, No. 4, pp. 599-612, 2013.

DorMohammadi, S., "Multilevel Design Optimization Under Uncertainty with Application to Product-Material Systems," Ph. D. Dissertation, Dept. of Aerospace Engineering, Mississippi State Univ., Starkville, MS, 2013.

DorMohammadi, S., Rais-Rohani, M., and Rouhi, M., "Hierarchical Analysis and Optimization of Nano-Enhanced Composite Sandwich Plates," Proceedings of the 16th AIAA Non-Deterministic Approaches Conference, National Harbor, MD, Jan. 13-17, 2014.

DorMohammadi, S., Rais-Rohani, M., and Rouhi, M., "Multilevel Design Optimization with Application to Material-Product Systems," Proceedings of the 10th AIAA Multidisciplinary Design Optimization Conference, National Harbor, MD, Jan. 13-17, 2014.

Du, X., and Chen, W., "Sequential Optimization and Reliability Assessment Method for efficient Probabilistic Design," Proceedings of the 2002 ASME Design Engineering Technical Conferences, Montreal, Canada, Sept. 29 - Oct. 2, 2002.

Dubois, D. and Prade, H., *Possibility Theory: An Approach to Computerized Processing of Uncertainty*, Plenum Press, New York, 1988.

Enevoldsen, I. and Sorensen, J. D., "Reliability-Based Optimization in Structural Engineering," *Structural Safety*, Vol. 15, pp. 169-196, 1994.

Federal Aviation Regulation, Part 25, Federal Aviation Administration, United States Department of Transportation, 2014.

Garcelon, J.H., Balabanov, V., and Sobieszczanski-Sobieski, J. "Multidisciplinary Optimization of a Transport Aircraft Wing Using VisualDOC," Proceedings of 40th Structures, Structural Dynamics, and Materials Conference, April 12-15, 1999.

Kim, H.M., Kokkolaras, M., Louca, L.S., Delagrammatikas, G.J., Michelena, N.F., Filipi, Z.S., Papalambros, P.Y., Stein, J.L., and Assanis, D.N., "Target Cascading in Vehicle Redesign: a Class VI Truck Study," *Int. J. Vehicle Design*, Vol. 29, No. 3, pp. 199-225, 2002.

Kim, H.M., Michelena, N.F., Papalambros, P.Y., and Jiang, T., "Target Cascading in Optimal System Design," *Journal of Mechanical Design*, Vol. 125, No. 3, pp. 474 – 480, 2003.

Kim, H.M., Chen, W., and Wiecek, M.M., "Lagrangian Coordination for Enhancing the Convergence of Analytical Target Cascading," *AIAA J*ournal, Vol. 44, No. 10, pp. 2197–2207, 2006.

Klir, G.J., and Smith, R.M., "On Measuring Uncertainty and Uncertainty- Based Information: Recent Developments," *Annals of Mathematics and Artificial Intelligence*, Vol. 32, No. 1, pp. 5 – 33, 2001.

Kokkolaras, M., Mourelatos, Z.P., and Papalambros, P.Y., "Design Optimization of Hierarchically Decomposed Multilevel Systems under Uncertainty," Proceedings of the 2004 ASME Design Engineering Technical Conferences, Salt Lake City, UT, Sept. 28 – Oct. 2, 2004.

Liu, H., Kokkolaras, M., Kim, H.M., Papalambros, P.Y., and Chen, W., "Probabilistic Analytical Target Cascading: a Moment Matching Formulation for Multilevel Optimization under Uncertainty," *Journal of Mechanical Design*, Vol. 128, No. 4, pp. 991-1000, 2006.

Louca, L.S., Kokkolaras, M., Delagrammatikas, G.J., Michelena, N.F., Filipi, Z.S., Papalambros, P.Y., and Assanis, D.N., "Analytical Target Cascading for the Design of an Advanced Technology Heavy Truck," Proceedings of the 2002 ASME International Mechanical Engineering Congress and Exposition, New Orleans, LA, Nov. 17-22, 2002.

McDowell, D.L., "Simulation-Assisted Materials Design for the Concurrent Design of Materials and Products," *JOM*, Vol. 59, No. 9, pp. 21-25, 2007.

Michalek, J.J., and Papalambros, P.Y., "An Efficient Weighting Update Method to Achieve Acceptable Consistency Deviation in Analytical Target Cascading," *Journal of Mechanical Design,* Vol. 127 pp. 206–214, 2005.

Michelena, N.F., Kim, H.M., and Papalambros, P.Y., "A System Partitioning and Optimization Approach to Target Cascading," Proceedings of the 12th International Conference on Engineering Design, Munich, Germany, 1999.

Mourelatos, Z.P. and Zhou, J., "A Design Optimization Method Using Evidence Theory," *Journal of Mechanical Design*, Vol. 128, No. 4, pp. 901 – 908, 2006.

MSC Nastran, Software Package, Ver. 2013.1 Student, MSC Software Corp., Newport Beach, CA, 2013.

Nemat-Nasser, S., and Hori, M., *Micromechanics: Overall Properties of Heterogeneous Solids*, North-Holland, Amsterdam, 1993.

Nikolaidis, E., Chen, S., Cudney, H., Haftka, R.T., and Rosca, R., "Comparison of Probability and Possibility for Design Against Catastrophic Failure Under Uncertainty," *Journal of Mechanical Design*, Vol. 126, No. 3, pp. 386-394, 2004.

Ostrower, J., "Is a Chinese Order for CSeries Imminent" *Flightglobal,* 1 Apr. 2010.

Parrish, J.C., "Reduced Order Techniques for Sensitivity Analysis and Design Optimization of Aerospace Systems," Ph.D. Dissertation, Dept. of Aerospace Engineering, Mississippi State Univ., Starkville, MS, 2014.

Pope, G.G., "The Buckling of Plates Tapered in Planform" *Royal Aircraft Establishment Farnborough*, Structures Report No. 274, 1964.

Rais-Rohani, M., and Marcellier, P., "Buckling and Vibration Analysis of Composite Sandwich Plates with Elastic Rotational Edge Restraints," *AIAA Journal*, Vol. 37, No. 5, pp. 579-587, 1999.

Rao, S.S., *Engineering Optimization: Theory and Practice*, 3rd ed., John Wiley and Sons, Hoboken, NJ, 1996.

Rouhi, M., Rais-Rohani, M., Lacy, T., Garg, M., and Abdi, F., "Mechanical Characterization of Nanofiber Enhanced Polymer with Application to Composite Crush Tubes," Proceedings of the 51st AIAA/ASME/ASCE/AHS/ASC Structures, Structural Dynamics, and Materials Conference, Orlando, FL, Apr 12-15, 2010.

Rouhi, M., "Modeling and Optimization of Nano-Enhanced Polymer Composite Structures Under Uncertainty," Ph.D. Dissertation, Dept. of Aerospace Engineering, Mississippi State Univ., Starkville, MS, 2011.

Rouhi, M., and Rais-Rohani, M., "Modeling and Probabilistic Design Optimization of a Nanofiber Enhanced Composite Cylinder for Buckling", 2013.

Salehghaffari, S. and Rais-Rohani, M., "Evidence-Based Design Optimization of Energy Absorbing Components under Material Field Uncertainty*,"* Proceedings of the 8th AIAA Multidisciplinary Design Optimization Specialist Conference, Honolulu, HI, Apr 23-26, 2012.

Shafer, G., *A Mathematical Theory of Evidence*, Princeton University Press, Princeton, NJ, 1976.

Sloan, J., "A400M Wing Assembly: Challenge of Integrating Composites," *High-Performance Composites*, p. 26, Jan 2013.

Timoshenko, S.P., and Gere, J.M., *Theory of Elastic Stability*, 2nd ed., McGraw-Hill, New York, 1961.

Tosserams, S., "Analytical Target Cascading: Convergence Improvement by Sub-Problem Post-Optimality Sensitivities," M.Sc. Thesis, Mechanical Engineering Dept., Eindhoven University of Technology, Eindhoven, Netherlands, 2004.

Tosserams, S., Etman, L.F.P., Papalambros, P.Y., and Rooda, J.E., "An augmented Lagrangian relaxation for analytical target cascading using the alternating direction method of multipliers," *Structural and Multidisciplinary Optimization*, Vol. 31, No. 3, pp.176-189, 2006.

Tosserams, S., Etman, L.F.P., and Rooda, J.E., "An Augmented Lagrangian Decomposition Method for Quasi-Separable Problems in MDO," *Structural and Multidisciplinary Optimization*, Vol. 34, No. 3, pp. 211-227, 2007.

Tu, J., Choi, K. K., and Park, Y. H., "A New Study on Reliability Based Design Optimization," *Journal of Mechanical Design*, Vol. 121, No. 4, pp. 557–564, 1999

Vasile, M., "Robust Mission Design Through Evidence Theory and Multiagent Collaborative Search," *Annals of the New York Academy of Sciences*, Vol. 1065, pp. 152-173, 2005.

Venter, G. and Sobieszczanski-Sobieski, J. "Multidisciplinary Optimization of a Transport Aircraft Wing Using Particle Swarm Optimization" *Structural and Multidisciplinary Optimization*, Vol. 26 Iss. 1-2, pp. 121-131, 2004.

Venter, G. and Sobieszczanski-Sobieski, J. "A Parallel Particle Swarm Optimization Algorithm Accelerated by Asynchronous Evaluations" *Journal of Aerospace Computing, Information, and Communication*, vol. 3, pp. 123-137, Mar. 2006.

Vinson, J.R., and Sierakowski, R.L., *The Behavior of Structures Composed of Composite Materials*, Martinus Nijhoff, Boston, 1986.

VisualDOC, Software Package, Ver. 7.1, Vanderplaats R&D, Colorado Springs, CO, 2012.

Winkler, R.L., *Introduction to Bayesian Inference and Decision*, Holt Rienhart and Winston, 1972.

Wittrick, W.H., "Buckling of Oblique Plates with Clamped Edges under Uniform Compression," *Aeronautical Quarterly*, Vol. 9, pp. 151-163, 1953.

Youn, B.D. and Wang, P., Bayesian Reliability-Based Design Optimization Under Both Aleatory and Epistemic Uncertainties, Proceedings of 11th AIAA/ISSMO Multidisciplinary Analysis and Optimization Conference, Portsmouth, VA, Sep 6-8, 2006.

Youn, B.D., Choi, K.K., Du, L., and Gorsich, D., "Integration of Possibility Based Optimization and Robust Design for Epistemic Uncertainty," *Journal of Mechanical Design*, Vol. 129, Issue 8, pp. 876–882, 2007.

Zadeh, L.A., "Fuzzy Sets," *Information and Control*, Vol. 8, No. 3, pp. 338 – 353, 1965.